Retrograde Lipid Traffic in Yeast: Identification of Two Distinct Pathways for Internalization of Fluorescent-labeled Phosphatidylcholine from the Plasma Membrane

Leslie S. Kean,* Robert S. Fuller,‡ and J. Wylie Nichols*

*Department of Physiology, Emory University School of Medicine, Atlanta, Georgia 30322; and ‡Department of Biochemistry, B400, Beckman Center, Stanford University School of Medicine, Stanford, California 94305-5307

Abstract. Digital, video-enhanced fluorescence microscopy and spectrofluorometry were used to follow the internalization into the yeast *Saccharomyces cerevisiae* of phosphatidylcholine molecules labeled on one acyl chain with the fluorescent probe 7-nitrobenz-2-oxa-1,3-diazol-4-yl (NBD). Two pathways were found: (1) transport by endocytosis to the vacuole and (2) transport by a non-endocytic pathway to the nuclear envelope and mitochondria.

The endocytic pathway was inhibited at low temperature (<2°C) and by ATP depletion. Mutations in secretory (*SEC*) genes that are necessary for membrane traffic through the secretory pathway (including *SEC1*, *SEC2*, *SEC4*, *SEC6*, *SEC7*, *SEC12*, *SEC14*, *SEC17*, *SEC18*, and *SEC21*) almost completely blocked endocytic uptake. In contrast, mutations in the *SEC63*, *SEC65*, or *SEC11* genes, required for translocation of nascent secretory polypeptides into the ER or signal peptide processing in the ER, only slightly reduced endocytic uptake. Phospholipid endocytosis was also independent of the gene encoding the clathrin heavy chain, *CHC1*. The correlation of biochemical analysis with fluorescence microscopy indicated that the fluorescent phosphatidylcholine was degraded in the vacuole and that degradation was, at least in part, dependent on the vacuolar proteolytic cascade.

The non-endocytic route functioned with a lower cellular energy charge (ATP levels 80% reduced) and was largely independent of the *SEC* genes. Non-endocytic transport of NBD-phosphatidylcholine to the nuclear envelope and mitochondria was inhibited by pretreatment of cells with the sulfhydryl reagents N-ethylmaleimide and p-chloromercuribenzenesulfonic acid, suggesting the existence of protein-mediated transmembrane transfer (flip-flop) of phosphatidylcholine across the yeast plasma membrane.

These data establish a link between lipid movement during secretion and endocytosis in yeast and suggest that phospholipids may also gain access to intracellular organelles through non-endocytic, protein-mediated events.

ALTHOUGH membranes of eukaryotic cells are composed of numerous classes of lipids, no membrane system can synthesize all of its lipid components (Pagano, 1990*a*). Thus, the transport and sorting of lipid molecules are important processes in the cell, and can affect both the homeostasis of organelles, and the regulation of other cellular processes such as endocytosis and secretion. Transport and sorting of lipids occurs via many intracellular pathways (for reviews see Pagano, 1990*a*,*b*; Pagano and Sleight, 1985; Bishop and Bell, 1988; van Meer, 1989). Anterograde transport pathways direct newly synthesized lipids to proper cellular destinations. These pathways can be either vesicular or non-vesicular, following the same pathways as protein secretion in some instances and independent pathways in others (Novick and Schekman, 1979; Sleight and Pagano, 1983; Urbani and Simoni, 1990). Transport of lipids also occurs through recycling pathways. One membrane recycling pathway that may carry out unique cellular functions is the transport of lipids from the plasma membrane to the intracellular organelles. Retrograde lipid transport can occur either by endocytosis, which allows both membrane-bound and soluble molecules to reach intracellular organelles (Koval and Pagano, 1990; Sleight and Pagano, 1984; Sleight and Abanto, 1989), or by protein-mediated transmembrane transport (flip-flop) followed by diffusion, perhaps facilitated by lipid transfer proteins, to intracellular organelles (van Meer and Op den Kamp, 1982; Sleight and Pagano, 1985; Martin and Pagano, 1987). Transmembrane flip-flop of lipids is important for the creation and maintenance of an asymmetric lipid composition across the bilayer. Such asymmetry has been shown to be an important indicator of the state of activation of platelets, in that the transbilayer distribution of the aminophospholipids changes dramatically when platelets undergo

Please address all correspondence to Dr. J. Wylie Nichols, Department of Physiology, Emory University School of Medicine, Atlanta, GA 30322.

their characteristic morphological and functional changes during activation (for review see Schroit and Zwaal, 1991). The proteins responsible for both types of retrograde lipid flow promise to be important players in many cellular sorting pathways, but, by and large, remain to be identified.

In mammalian cells, retrograde lipid transport pathways have been studied using fluorescent phospholipid analogs (Pagano and Sleight, 1985). Diacylated lipids with a fluorescent, 7-nitrobenz-2-oxa-1,3-diazol-4-yl (NBD)[1]-labeled aminocaproic acid in place of one fatty-acyl chain can be transferred to the plasma membrane at low temperature and thus serve as powerful tools for dissecting both the endocytic and non-endocytic phospholipid internalization pathways (Pagano, 1990*a*; Struck and Pagano, 1980). Internalization of fluorescent phospholipids depends both on their polar head-group and on cell-type. NBD-labeled phosphatidylcholine is internalized exclusively through endocytosis in untransformed mammalian cell lines, and is targeted either to the Golgi apparatus, or to endosomes (Sleight and Pagano, 1984; Sleight and Abanto, 1989). In VA-2 cells, which are SV40-transformed human lung fibroblasts, NBD-labeled phosphatidylcholine is internalized both by endocytosis to the Golgi apparatus, and by flip-flop from the outer to inner leaflets of the plasma membrane before transferring to the nuclear envelope and mitochondria (Sleight and Abanto, 1989). In chinese hamster V79 fibroblasts, NBD-labeled phosphatidylethanolamine is internalized both by endocytic and protein-mediated, non-endocytic mechanisms (Sleight and Pagano, 1985; Martin and Pagano, 1987). Endocytosis delivers this molecule to the Golgi apparatus. The non-endocytic pathway targets the lipid to both the nuclear envelope and the mitochondria. In contrast, NBD-labeled phosphatidylserine is internalized exclusively through protein-mediated flip-flop, and is transported to the nuclear envelope and mitochondria of V79 fibroblasts (Martin and Pagano, 1987). Thus, pathways taken by phospholipids in mammalian cells appear to be both head-group specific and cell-type specific. One general rule appears to be followed, namely, endocytic uptake delivers lipids to the Golgi and endosomal/lysosomal system, whereas flip-flop-mediated uptake principally targets lipids to the nuclear envelope and mitochondria.

The importance of lipid trafficking events for cell viability has been highlighted recently by studies of *Saccharomyces cerevisiae* (yeast). Riezman (1985) has shown that yeast internalize the aqueous marker, Lucifer yellow, by fluid phase endocytosis and transport it specifically to the vacuole (the yeast lysosome). Endocytosis of this "content-marker" depends on several of the essential *SEC* gene products that include Sec7p, which is associated with intra-Golgi transport vesicles (Franzusoff and Schekman, 1989; Franzusoff et al., 1992). The *SEC14* gene, required for formation of secretory vesicles from the Golgi (Novick et al., 1981; Stevens et al., 1982) encodes a phosphatidylcholine-phosphatidylinositol transfer protein (Bankaitis et al., 1990), suggesting that the maintenance of the correct organellar lipid composition may be essential for viability. *SEC14* mutations also inhibit the delivery of Lucifer yellow to the vacuole by ~50% (Riezman, 1985), suggesting that regulation of lipid composition and trafficking may be crucial for both endo- and exocytosis. The fact that many mutants originally isolated for their secretory defects are also deficient in fluid phase endocytosis suggests either that such proteins function in both pathways, or that secretory and endocytic events are obligatorily coupled.

Recently, mutations in two genes, *END3* and *END4*, have been isolated for their defect in receptor-mediated endocytosis of the mating pheromone α-factor into *MATa* haploids. Although mutations in these genes also inhibit endocytosis of Lucifer yellow, they have no effect on secretion (Raths et al., 1993). Thus the pathways of receptor-mediated endocytosis and secretion do exhibit some independence.

In this study, we have used fluorescent-labeled phosphatidylcholine (M-C_6-NBD-PC) to follow retrograde lipid transport in *S. cerevisiae*. We present evidence for two distinct lipid traffic pathways. One has the characteristics of a classic endocytic pathway, results in phospholipid transport to the vacuole, and requires the activities of at least 10 *SEC* genes. The other pathway is largely *SEC* gene-independent, and transports phospholipids to the nuclear envelope and mitochondria, characteristic of a transmembrane transport (flip-flop) process.

Materials and Methods

Materials

Yeast media was from Difco Labs. (Detroit, MI). Unless otherwise noted, all other materials were purchased from Sigma Chem. Co. (St. Louis, MO).

Yeast Strains and Culture

The *S. cerevisiae* strains used are shown in Table I. For all experiments, early to mid log-phase cultures (OD_{600} = 0.2-1) were grown from either overnight cultures or fresh plates in synthetic complete media (SDC) as described (Sherman et al., 1986). Wild-type strains were typically grown at 30°C. Temperature-sensitive (Ts^-) strains were grown at a permissive temperature of 22–24°C.

Vesicle Preparation

1-myristoyl-2-[6-[(NBD)amino]caproyl]phosphatidylcholine (M-C_6-NBD-PC), dioleoylphosphatidylcholine (DOPC), and dioleoylphosphatidylethanolamine were from Avanti Polar Lipids Inc. (Alabaster, AB). N-Rhodamine-dioleoylphosphatidylethanlamine (N-Rh-DOPE) was synthesized and purified as described (Struck et al., 1981). Phospholipids were stored at −20°C, periodically monitored for purity by thin-layer chromatography, and repurified when necessary. Phospholipid concentrations were determined by the lipid phosphorus assay (Ames and Dubin, 1960). To prepare vesicles, lipids were first mixed in desired proportions and the chloroform removed by evaporation under nitrogen followed by overnight vacuum desiccation. Desiccated lipids were then solubilized in SDC medium lacking glucose and the mixture passed seven times through a Lipex Extruder (Lipex Biomembranes Inc., Vancouver, BC, Canada) equipped with 0.1-μm filters to produce vesicles. Total lipid concentration in the stock vesicle preparation was 1 mM. Typically, proportions were 40 mol% M-C_6-NBD-PC, 2 mol% N-Rh-DOPE, 58 mol% DOPC.

1. *Abbreviations used in this paper*: DAPI, 4',6-diamidino-2 phenylindole; DIC, differential interference contrast; DOPC, dioleoylphosphatidylcholine; M-C_6-NBD-PC, 1-myristoyl-2-[6-(NBD) amino]caproyl]phosphatidylcholine; NaN_3, sodium azide; NBD, 7-nitrobenz-2-oxa-1,3-diazol-4-yl; NEM, N-ethylmaleimide; N-Rh-DOPE, N-Rhodamine-dioleoylphosphatidylethanolamine; pCMBS, para-chloromercuribenzenesulfonic acid; Rh, rhodamine; $SCNaN_3$, synthetic complete media lacking glucose but containing 2% sorbitol and 20 mM sodium azide; SDC, synthetic complete media; *SEC*, secretory; Ts−, temperature-sensitive; wt, wild-type.

Table I. Yeast Strains Used in This Study

Strain	Genotype	Source
CRY3*	*(MATa Sec⁺ can1-100 ade2-1 his2-11,15 leu2-3-112 trp1-1 ura3-1)* (MATα *Sec⁺ can1-100 ade2-1 his2-11,15 leu2-3-112 trp1-1 ura3-1)*	R. S. Fuller lab collection
CRY1*	*(MATa Sec+ can1-100 ade2-1 his2-11,15 leu2-3-112 trp1-1 ura3-1)*	R. S. Fuller lab collection
CBO18*	*(MATa Sec+ can1-100 ade2-1 leu2-3-112 trp1-1 ura3-1 pep4Δ:HIS3 prb1Δ::hisG prc1Δ::hisG)*	R. S. Fuller lab collection
KRY30-2C*	*(MATa sec1-1 can1-100 ade2-1 his2-11,15 leu2-3-112 trp1-1)*	R. S. Fuller lab collection
KRY31-3C*	*(MATa sec7-1 sec1-1 can1-100 ade2-1 his2-11,15 leu2-3-112 trp1-1)*	R. S. Fuller lab collection
CWS11-2*	*(MATa sec11 ade2-1 his2-11,15 leu2-3-112 trp1-1 ura3-1)*	R. S. Fuller lab collection
CRY2*	*(MATα Sec+ can1-100 ade2-1 his2-11,15 leu2-3-112 trp1-1 ura3-1)*	R. S. Fuller lab collection
KRY33-2C*	*(MATα sec14 can1-100 ade2-1 his2-11,15 leu2-3-112 trp1-1 ura3-1)*	R. S. Fuller lab collection
CWS18-1*	*(MATα sec18 can1-100 ade2-1 his2-11,15 leu2-3-112 trp1-1 ura3-1)*	R. S. Fuller lab collection
X2180-1A	*(MATa Sec+ SUC2 mal gal2 CUP1)*	Yeast Genetic Stock Center
HMSF106	*(MATa sec2-56 SUC2 mal gal2 CUP1)*	Yeast Genetic Stock Center
HMSF13	*(MATa sec4-2 SUC2 mal gal2 CUP1)*	Yeast Genetic Stock Center
SF266-1C	*(MATa sec12-4 SUC2 mal gal2 CUP1)*	Yeast Genetic Stock Center
HMSF175	*(MATa sec17-1 SUC2 mal gal2 CUP1)*	Yeast Genetic Stock Center
HMSF180	*(MATa sec21-1 SUC2 mal gal2)*	Yeast Genetic Stock Center
X2180-1B	*(MATα Sec+ SUC2 mal gal2 CUP1)*	Yeast Genetic Stock Center
RSY153	*(MATα sec63-1 leu2-3,-112 ura3-52)*	R. Schekman, UC Berkeley
RSY457	*(MATα sec65 ade2 his3 leu2-3,-112 trp1-1 ura3-52)*	R. Schekman, UC Berkeley
NY13	*(MATa; Sec+ ura3-52)*	P. Novick, Yale U.
NY17	*(MATa; sec6-4 ura3-52)*	P. Novick, Yale U.
GPY55	*(MATα CHC1 leu2-3-112 ura3-52 his4 trp1 prb1)*	G. Payne, UCLA
GPY184	*(MATα chc1-52 leu2-3-112 ura3-52 his4 trp1 prb1)*	G. Payne, UCLA

* Strains were derived from a nominally isogenic pair of strains, W303-1A (*MATa can1-100 ade2-1 his2-11,15 leu 2-3-112 trp1-1*) and W303-1B (W303-1A *MATα*) originally obtained from R. Rothstein, Columbia University.

Internalization of Phospholipids into Yeast Cells

For internalization assays using non-Ts− strains, logarithmically growing cells were harvested by centrifugation and washed twice with either SDC or $SCNaN_3$ (SDC medium lacking glucose but containing 2% sorbitol and 20 mM sodium azide). In the azide-containing cultures, cells were incubated with shaking for 45–50 min at 30°C to deplete cellular ATP stores. For fluorescence microscopy, 1.5 ml of cells were mixed with vesicles (50 μM total lipid concentration) and incubated at 30°C or 2°C for 1.5–2 h with constant (30°) or intermittent (2°) shaking. Cells were then rapidly moved to an ice-water bath, washed rapidly four times with two volumes ice-cold $SCNaN_3$ and viewed under the microscope. For experiments with Ts− strains, both growth to log-phase and ATP depletion were carried out at 24°C. Cultures were then split, and half of the cells were warmed to the restrictive temperature of 37°C, while the other half remained at 24°C. Warming to 37°C was accomplished by shifting the temperature of the shaking water bath up to 37°C, resulting in a complete change of temperature in ~10 min. After shifting the temperature for 30 min, vesicles were added and incubation at 37°C was continued for 1 h. Cells that were kept at the permissive temperature (24°C) were incubated with vesicles for 2 h. Cells were then plunged into an ice-water bath and washed rapidly with ice-cold $SCNaN_3$ in preparation for microscopy. In experiments involving Ts− mutants, control strains were handled identically to the mutants. For fluorometry, 1.9 ml of cells were placed in a fluorescence cuvette (preequilibrated to the proper temperature) and stirred continuously with a magnetic stirrer. Vesicles were then added (50 μM total lipid) and the change in fluorescence was monitored continuously.

Measurement of ATP Levels

ATP was measured using the Luciferase assay on cells incubated in either glucose-rich medium (SDC) or ATP depletion medium ($SCNaN_3$). After ATP depletion, cells were centrifuged for 25 min at 1,500 *g* to yield a well-packed cell-paste, 50 μl of which was diluted into 0.9 ml of 7% PCA and incubated on ice for 15 min. Extracts were centrifuged for 5 min at 4°C in a microfuge at maximum speed. 100 μl of the supernatant was added to 0.5 ml luciferase assay buffer (5 mM sodium arsenate, 4 mM magnesium sulfate, 20 mM glycylglycine, pH 8.0) and the pH was adjusted to 8–9 by adding 1.47 N KOH in 25 mM Tris, pH 8.0 (~90 μl). 50 μl of pH-adjusted extract was added to 0.9 ml of luciferase assay buffer, followed by the addition of 50 μl of luciferase/luciferin reagent (supplied at 20 mg/ml). Luminescence was measured using a Packard TriCarb Liquid Scintillation Spectrometer.

Catabolism of M-C_6-NBD-PC in Yeast

To study the degradation of M-C_6-NBD-PC, internalization assays were performed as described above. Equal numbers of cells were harvested and frozen at −80°C for at least 1 h. Extraction of cellular lipids was performed as described (Hjelmstad and Bell, 1987). After extraction, the aqueous and organic phases were evaporated under nitrogen (equal volumes of acetonitrile were added to the aqueous fraction to facilitate evaporation), and resuspended in chloroform (organic phase) or chloroform/methanol, 1:1 (aqueous phase). A portion of this was separated by silica gel TLC (Merck Inc., Germany) in chloroform/methanol acetone/acetic acid/water, 5:1:2:1:0.5 (Struck and Pagano, 1980), and viewed on an ultraviolet transilluminator.

Relative Internalization of M-C_6-NBD-PC and N-Rh-DOPE

Lipids were extracted from yeast cells as described above, the organic phase was evaporated, and the lipids were resuspended in 2 ml chloroform/methanol, 1:1. NBD and rhodamine fluorescence was measured using an SLM 8000C spectrofluorometer as described below. To quantify internalization of NBD-labeled lipids, the NBD signal was compared to a standard curve of M-C_6-NBD-PC in chloroform/methanol, 1:1.

N-ethylmaleimide and para-chloromercuribenzenesulfonic Acid Sensitivity Experiments

Mid-log phase cells were prepared as described above, cooled to 2°C, har-

vested by centrifugation and resuspended in buffered media (SDC containing 50 mM sodium phosphate buffer, pH 7.5) containing either 2 mM *N*-ethylmaleimide (NEM), 10 mM para-chloromercuribenzenesulfonic acid (pCMBS), or 50 mM pCMBS. Cells were incubated on ice for 30 min and were shaken after the first 15 min. Cells recovered by centrifugation were resuspended in buffered medium (for pCMBS experiments), or buffered medium containing 2 mM dithiothreitol (for NEM experiments), and incubated on ice for 5 min. Cells were pelleted again, washed once with buffered medium, and resuspended in buffered media with 50 μM M-C_6-NBD-PC-containing vesicles. Cells were incubated on ice for 1.5 h, and washed three times with ice-cold $SCNaN_3$ buffered with 50 mM sodium phosphate (pH 7.5) before fluorescence microscopy.

Fluorescence Measurements

Fluorescence was recorded using a MPF-44E fluorescence spectrophotometer (Perkin-Elmer Corp., Norwalk, CT) or from an SLM 8000C spectrofluorometer (SLM Instruments Inc., Urbana, IL). Temperature was controlled with a circulating water bath. Analogue output from the Perkin-Elmer fluorometer was digitized and stored on an IBM-XT. Digital output from the SLM 8000C was stored on an IBM-AT-compatible computer. NBD fluorescence was monitored by exciting the fluorophore at 475 nm, and reading emission at 530 nm. Rhodamine fluorescence was monitored by exciting the fluorophore at either 560 or 580 nm and reading the emission at 590 nm.

Fluorescence Microscopy

Fluorescence microscopy was performed on a Zeiss Axiovert microscope equipped with barrier filters that allowed no crossover of NBD and rhodamine fluorescence. For localization of 4',6-diamidino-2-phenylindole (DAPI) fluorescence, barrier filters were used that did not allow crossover of NBD and DAPI fluorescence. The fluorescence image was enhanced with a SIT 66 image-intensifying camera (DAGE-MTI Inc., Michigan City, IN), digitized, and stored on magnetic disks using an IBM-AT-compatible computer. Contrast enhancement and pixel brightness analysis of the digital images was performed with Image-1/AT software. Average pixel brightness was measured from a rectangle (1 × 3 pixels) in the middle of vacuoles or a rectangle (10 × 12 pixels) surrounding the nuclear envelope. Pixel brightness analysis of DOPC vesicles containing known amounts of M-C_6-NBD-PC confirmed that these measurements fell within the linear range of the SIT camera.

Statistical Analysis

Statistical analysis was performed with the InStat statistics software from GraphPad Inc. (San Diego, CA). χ^2 analysis and two-tailed P values were obtained for the vesicular-transport *sec* mutants after creating a 3 × 2 contingency table to compare the vacuolar pixel brightness values of the *sec* mutants and their isogenic Sec+ alleles. All pixel brightness measurements from the nonpermissive temperature (37°C) were corrected for strain-to-strain variations in vacuolar pixel brightness at the permissive temperature (24°C). The contingency tables were split into three pixel brightness bins, in which vacuolar pixel brightness scores were divided. The bins were for vacuolar pixel brightness values of 0, >0-20, and >20. These bins were chosen after examination of the pixel brightness ranges of both the vesicular-transport *sec* mutants and their isogenic Sec+ alleles. Many vesicular-transport *sec* mutants had vacuolar brightness values of 0 (their vacuoles were not fluorescent). The remaining cells had vacuoles with wide-ranging vacuolar pixel brightness, but the vast majority did not exceed a pixel brightness value of 20. The Sec+ strains had widely ranging pixel brightness values, with an average vacuolar pixel brightness of ~100. Because the ER *sec* mutants did not have any cells with vacuolar fluorescence of 0 (see Fig. 7), it was impossible to use the 3 × 2 contingency tables to perform the χ^2 test, and Fisher's Exact test was employed instead. For those experiments which yielded normal (Gaussian) pixel brightness distributions, the Student's *t* test was used to compare the means and calculate a two-tailed P value.

Results

Uptake of M-C_6-NBD-PC into Multiple Intracellular Organelles

When the diploid wild-type (wt) strain, CRY3, was incubated at 30°C in the presence of vesicles (50 μM total lipid concentration) containing 40 mol% M-C_6-NBD-PC, 2 mol% N-Rh-DOPE and 58 mol% DOPC, only the exchangeable fluorescent lipid, M-C_6-NBD-PC (Nichols, 1985), was internalized. M-C_6-NBD-PC was transported to the vacuole, identified by colocalization of NBD fluorescence with either the fluorescent vacuoles of *ade2* yeast (L. S. Weisman et al., 1987) (data not shown) or with vacuoles visualized by differential interference contrast (DIC) optics (Fig. 1, *A*, *B*, and *D*). A smaller amount of M-C_6-NBD-PC was incorporated into the nuclear envelope and the mitochondria, as identified by colocalization with vital DAPI-staining of DNA in these organelles (Fig. 1, *A* and *C*). Although the vacuolar fluorescence shown in Fig. 1 *A* obscures the mitochondrial fluorescence, in other experiments (data not shown), colocalization of NBD fluorescence with DAPI-labeled mitochondria was clear (see Fig. 3). The NBD-fluorescence of nuclei and mitochondria photobleached much more rapidly than did the vacuolar fluorescence. Fluorescent nuclei and mitochondria could be photographed after ~2 s of exposure to the excitation light (Fig. 1 *A*) but had faded almost entirely by 20 s of exposure, leaving the vacuole as the sole fluorescent organelle (Fig. 1 *B*). In fact, even when photographed after ~2 s, significant photobleaching of the nuclear envelope and mitochondria had occurred. Thus, although the fluorescence patterns shown in Fig. 1 *A* demonstrated that M-C_6-NBD-PC was transported both to the vacuole and to the nuclear envelope, the vacuolar destination is emphasized due to the fact that the vacuolar fluorescence photobleached more slowly than the fluorescence in the nuclear envelope and mitochondria.

Internalization Occurs after Incorporation of M-C_6-NBD-PC Monomers into the Plasma Membrane

Three possible mechanisms could account for the ability of cells to internalize M-C_6-NBD-PC. (1) The lipid could be internalized as part of an intact donor vesicle during endocytosis, or through fusion of the donor vesicles with the plasma membrane. (2) The lipids could be internalized as soluble monomers in the aqueous phase after dissociation from donor vesicles, and thus serve only as a content marker for endocytic events. (3) The lipids could be internalized as monomers after insertion into the plasma membrane of the cell, and thus serve as a marker for lipid traffic via both endocytic and non-endocytic pathways.

The first possibility was ruled out by the differential partitioning experiment shown in Table II. Previous studies have shown that while M-C_6-NBD-PC monomers can rapidly partition from donor vesicles ($t_{1/2}$ for dissociation ~2 s), N-Rh-DOPE dissociates from vesicles very slowly ($t_{1/2}$ for dissociation ~ days) (Nichols, 1985; Nichols and Pagano, 1983). Thus, internalization of M-C_6-NBD-PC monomers after incorporation into the plasma membrane can be distinguished from internalization of intact donor vesicles or fusion of donor vesicles with the plasma membrane by the extent to which M-C_6-NBD-PC is enriched in cells relative to N-Rh-DOPE. The extent of enrichment was determined from the ratio of NBD to rhodamine (Rh) fluorescence measured in a total lipid extract from cells vs the ratio measured in the extracted donor vesicles. As can be seen in Table II, the ratio of NBD to Rh fluorescence increased from 7.8 (in

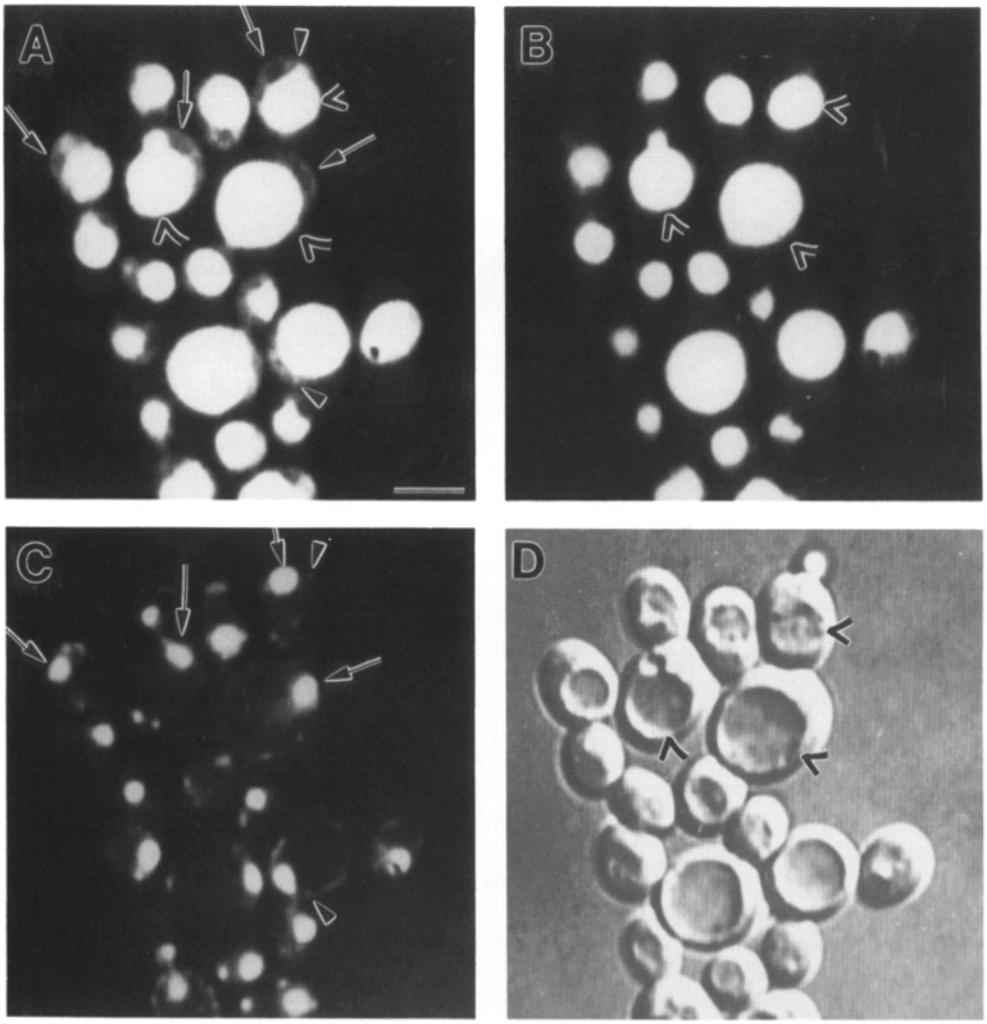

Figure 1. Digital image of CRY3 cells in which M-C_6-NBD-PC internalization assays were performed at 30°C in SDC. Internalization assays were performed on the diploid wt strain, CRY3, as described in Materials and Methods. In vivo DAPI labeling was performed by adding 2.5 μM DAPI for 1 h before microscopy. The panels show: (*A*) NBD fluorescence, digital image taken immediately after exposing the field of cells to excitatory light. (*B*) Same field as in *A* after ~20 s of continuous illumination of this field of cells (nuclear envelope and mitochondrial fluorescence photobleach preferentially, leaving only vacuolar fluorescence). (*C*) DAPI labeling of nuclear envelope and mitochondria (*D*) DIC optics. Open arrowheads point to representative vacuoles, closed arrowheads point to representative mitochondria, arrows point to representative nuclei. Bar, 5 μm.

vesicle extracts) to 330 (in cellular extracts) when CRY3 cells were incubated with vesicles under conditions that allowed internalization. Thus, at least ~98% of the fluorescence seen in CRY3 was due to the uptake of M-C_6-NBD-PC monomers.

As will be discussed in detail below, when total cellular lipids were extracted from CRY3 cells and separated by TLC, significant degradation of M-C_6-NBD-PC was observed only under conditions (incubation at 30°C in SDC medium) that allowed transport to the vacuole (Fig. 5). Because this degradation resulted in the production of molecules that did not partition into the organic phase of a lipid extraction (Table III), the NBD fluorescence signal used to determine the fold-enrichment of NBD fluorescence relative to Rh fluorescence after phospholipid internalization (which was measured from the organic phase of a lipid extraction of CRY3 cells) might be artifactually low. The experiment was repeated, therefore, with the strain CB018 (Pep−), which is isogenic to CRY3 (Pep+) except that it is a *MATa* haploid and lacks the three major vacuolar peptidases, proteases A and B and carboxypeptidase Y (CPY). The vacuoles of Pep− strains are largely devoid of hydrolytic activities, presumably including lipases (Jones, 1991; Takeshige et al., 1992). In this experiment, the ratio of NBD to Rh fluorescence was 3.3 for vesicles and 1900 for CB018 cells. Therefore, in CB018, at least 99.8% of M-C_6-NBD-PC uptake into the cells was independent of the uptake of intact donor vesicles.

Table II. Internalization of M-C_6-NBD-PC Does Not Occur Via Vesicle Adsorption

Strain	Ratio of NBD/Rh Fluorescence		% Fluorescence attributable to vesicle adsorption
	Vesicles	Cellular lipids	
CRY3	7.8	330	2%
CB018	3.3	1900	<<1%

Internalization assays were performed on either pep$^+$ (CRY3) or pep$^-$ (CB018) cells as described. The cells were washed free of donor vesicles, and lipids were extracted both from the cells and from the vesicle preparations themselves. Both NBD and Rh fluorescence were quantified.

The second possibility, that the fluorescence observed in the microscope was due to internalization of soluble M-C_6-NBD-PC monomers as part of the aqueous content of endocytic vesicles seems highly unlikely, based on the following experiment. Internalization assays were performed on CRY3 and CB018 under conditions allowing maximum lipid internalization. Total cellular lipids were then extracted, and the NBD fluorescence was compared to a standard curve for NBD fluorescence vs moles of M-C_6-NBD-PC. The total amount of NBD-labeled lipid internalized per OD unit for CRY3 and CB018 was 0.37 nmol and 0.65 nmol, respectively.

Table III. Degradation of M-C_6-NBD-PC Is Partially Inhibited in a Pep4⁻, Prb1⁻, Prc1⁻ Strain

Strain	Relevant genotype	Vacuolar fluorescence (Avg. pixel brightness of vacuoles in digital images) (arbitrary units)	Relative fluorescence of lipids separated by TLC*	
			M-C_6-NBD-PC	major aqueous catabolite
CRY3	*PEP4, PRB1, PRC1*	47	1	1.5
CB018	*pep4Δ::HIS3, prb1Δ::hisG, prc1Δ::hisG*	96	5	0.2

Internalization assays were performed on Pep⁺ (CRY3) or Pep⁻ (CB018) cells. The amount of vacuolar fluorescence was measured by quantifying the pixel brightness of the vacuoles seen in the digital images using the Image1/AT software system. Also, lipids were extracted from the cells, and separated by thin-layer chromatography (TLC). The spots corresponding to the starting material (M-C_6-NBD-PC) and the major aqueous catabolite were scraped, extracted from the silica support, and quantified spectrofluorometrically.

* The fluorescence intensities shown for the TLC-separated products are relative to the fluorescence intensity measured for M-C_6-NBD-PC from CRY3.

As described previously (Nichols, 1985), if we assume that all of the fluorescence that was measured arose from monomers of M-C_6-NBD-PC internalized in the aqueous phase, the equivalent number of internalized cell volumes required to account for the amount of uptake can be calculated from the following equation:

$$N_{vi} = (n/L_{aq})/V_c$$

where N_{vi} = number of cellular volumes internalized, n = nmol of M-C_6-NBD-PC per OD unit, L_{aq} = concentration of fluorescent lipid in the aqueous phase, and V_c = the volume of packed cells per OD unit. The concentration of the fluorescent phospholipids in the aqueous phase in equilibrium with vesicles can be calculated by dividing the mole fraction of M-C_6-NBD-PC in the donor vesicles (0.4) by the equilibrium constant for its association with these vesicles (9.8×10^6 M^{-1}) (Nichols, 1985). Thus, the concentration of M-C_6-NBD-PC in the aqueous phase at equilibrium (L_{aq}) for a typical experiment is 4×10^{-8} M. Given that the volume of packed cells per OD unit was 3.9 μl (CRY3) and 3.4 μl (CB018), we calculate that the two strains would have had to internalize a minimum of 2400 (CRY3) and 4800 (CB018) times their cellular volumes in the two hour recording time (20 cell vol per min and 40 cell vol per min, respectively) if the intracellular fluorescence signal arose from the internalization of lipid monomers in the aqueous phase. It seems highly improbable that yeast turn-over their cellular volume at such a high rate, and thus highly unlikely that the fluorescence signal is due to internalization of lipid monomers in the aqueous phase. Thus, having eliminated the possibility that cells internalize M-C_6-NBD-PC (1) as part of an intact donor vesicle, or (2) as a monomer in the aqueous phase, the most plausible mechanism for the uptake of M-C_6-NBD-PC by yeast cells is internalization of lipids that have inserted into the plasma membrane after dissociating from donor vesicles.

Temperature and Energy Dependence Distinguish Two Import Pathways

The effects of temperature and intracellular ATP levels on the internalization of M-C_6-NBD-PC were investigated. Microscopic analysis revealed that vacuolar accumulation of NBD fluorescence was blocked at 2°C, but labeling of the mitochondria and nuclear envelope still occurred (Fig. 2, *D*, *E*, and *F*, and Fig. 3, *A*, *B*, and *C*). Incubation of CRY3 in medium lacking a carbon source and containing 20 mM sodium azide ($SCNaN_3$ medium) for 45–50 min at 30°C decreased the intracellular ATP pools by 80% as determined by luciferase assays (data not shown). At 30°C, this degree of ATP-depletion inhibited traffic of M-C_6-NBD-PC to the vacuole, but did not interfere with transport to the nuclear envelope and mitochondria (Fig. 2, *A*, *B*, and *C* and Fig. 3, *D*, *E*, and *F*). As can be seen in Fig. 2, *B* and *E* mitochondria could not be labeled with DAPI when it was added either after ATP depletion (Fig. 2 *B*) or during incubation in SDC at 2°C (Fig. 2 *E*), although labeling of the nucleus still occurred. To confirm that M-C_6-NBD-PC was transported to the mitochondria under these incubation conditions, we first pretreated cells with DAPI at 30°C in SDC (which allowed both the nuclei and mitochondria to be labeled) before depleting ATP stores or lowering the incubation temperature to 2°C and adding M-C_6-NBD-PC-containing donor vesicles. With this procedure, we were able to confirm the nuclear envelope- and mitochondrial-location of the NBD fluorescence both when the incubation temperature was lowered to 2°C and under conditions of ATP depletion (Fig. 3). When the incubation temperature was lowered to 2°C in cells that had undergone ATP depletion, traffic not only to the vacuole, but also to the nuclear envelope and mitochondria was completely blocked (Fig. 2, *G*, *H*, and *I*). Inhibition of traffic to the vacuole with continued traffic to the nuclear envelope and mitochondria when cells were incubated at 30°C in $SCNaN_3$ or at 2°C in SDC suggested that internalization to the vacuole occurred by an endocytic pathway (Anderson et al., 1977; Draper and Simon, 1980; Helenius et al., 1980), and internalization to the nuclear envelope and the mitochondria resulted from non-endocytic events.

Since a fluorescence signal occurred only upon internalization of M-C_6-NBD-PC, the rate of internalization could be measured as the rate of increase in fluorescence in real time in the spectrofluorometer. Fig. 4 shows that this increase in fluorescence signal with time depended on temperature and intracellular ATP. Incubation of cells at 30°C in normal growth medium (shown in the trace labeled "30°C, SDC" in Fig. 4), resulted in a rapid increase in fluorescence

Figure 2. Digital image of CRY3 cells in which M-C_6-NBD-PC internalization assays were performed under inhibitory conditions. Internalization assays were performed on the diploid wild-type strain, CRY3 under conditions that disturbed the lipid traffic pathways shown in Fig. 1. (*A–C*) Cells incubated at 30°C after incubation in $SCNaN_3$ medium to deplete ATP. (*D–E*) Cells incubated at 2°C in SDC.

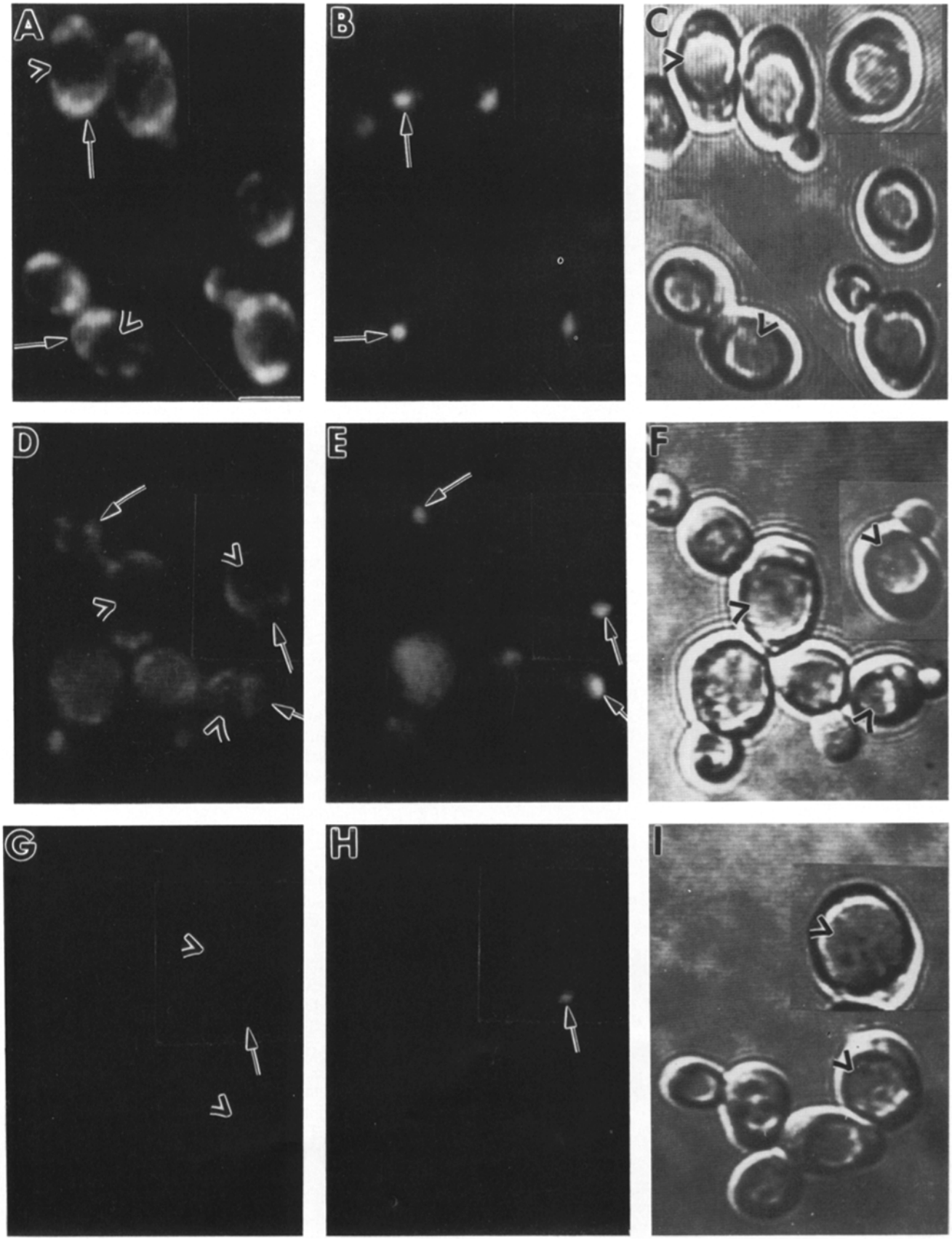

(*G–I*) Cells incubated at 2°C after incubation in $SCNaN_3$ medium to deplete ATP. (*A*) NBD fluorescence; (*B*) DAPI fluorescence; (*C*) DIC optics; (*D*) NBD fluorescence; (*E*) DAPI fluorescence; (*F*) DIC optics; (*G*) NBD fluorescence; (*H*) DAPI fluorescence; (*I*) DIC optics. Open arrowheads point to representative vacuoles, arrows point to representative nuclei. Bar, 5 μm.

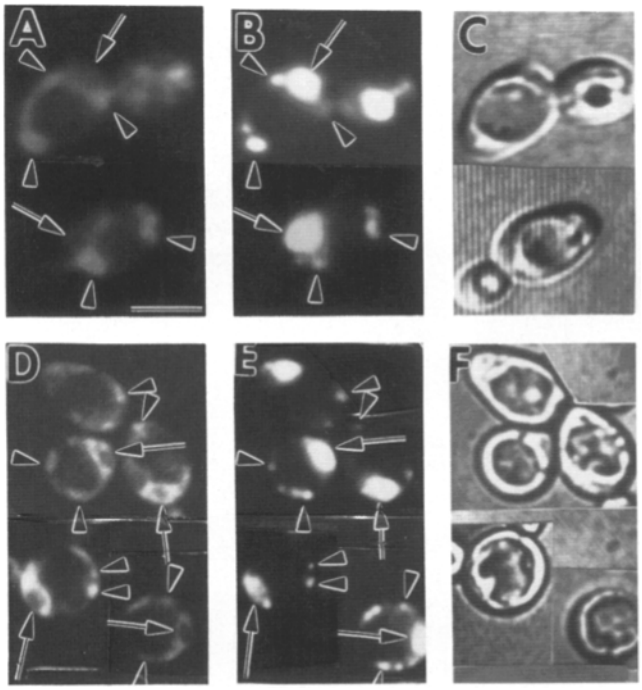

Figure 3. Digital image of CRY3 cells in which M-C_6-NBD-PC internalization assays were performed at 2°C in SDC and at 30°C in $SCNaN_3$. The cells were preincubated with 2.5 μM DAPI for 1 h at 30°C in SDC before shifting the temperature to 2°C or depleting ATP levels and adding M-C_6-NBD-PC-containing vesicles. This pretreatment enhanced the fluorescence of DAPI-labeled mitochondria, and thus allowed the confirmation of the localization of NBD fluorescence to the nuclear envelope and mitochondria. (*A–C*) Cells incubated at 2°C in SDC. (*D–F*) Cells incubated at 30°C in $SCNaN_3$. (*A*) NBD fluorescence; (*B*) DAPI fluorescence; (*C*) DIC optics; (*D*) NBD fluorescence; (*E*) DAPI fluorescence; (*F*) DIC optics. Closed arrowheads point to representative mitochondria, arrows point to representative nuclei. Bar, 5 μm.

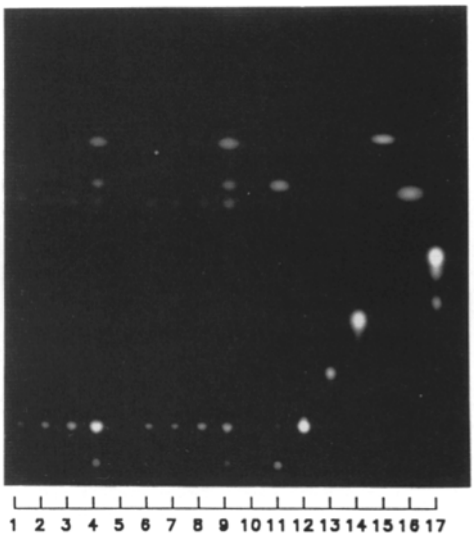

Figure 5. TLC analysis of fluorescent lipids extracted from CRY3 and CBO18 cells. Internalization assays were performed on CRY3 (Pep^+) and CBO18 (Pep^-) strains. Lipids were extracted from the cells as described in Materials and Methods. Solvent was evaporated under a nitrogen stream, and the lipids that partitioned into the organic phase of the extraction were resuspended in chloroform. Lipids from equal numbers of cells were spotted onto a TLC plate which was developed in chloroform/methanol/acetone/acetic acid/water, 5:1:2:1:0.5. The lanes show: (*1*) CBO18 cells incubated with donor vesicles in $SCNaN_3$ medium at 2°C. (*2*) CBO18 incubated with vesicles in SDC at 2°C. (*3*) CBO18 incubated with vesicles in $SCNaN_3$ at 30°C. (*4*) CBO18 incubated with vesicles in SDC at 30°C. (*5*) CBO18 in SDC at 30°C, incubated without vesicles. (*6*) CRY3 cells incubated with donor vesicles in $SCNaN_3$ at 2°C. (*7*) CRY3 incubated with vesicles in SDC at 2°C. (*8*) CRY3 incubated with vesicles in $SCNaN_3$ at 30°C. (*9*) CRY3 incubated with vesicles in SDC at 30°C. (*10*) CRY3 in SDC at 30°C, incubated without vesicles. (*11*) M-C_6-NBD-PC treated with phospholipase A_2. (*12*) M-C_6-NBD-PC standard. (*13*) M-C_6-NBD-phosphatidylethanolamine standard. (*14*) M-C_6-NBD-phosphatidic acid standard. (*15*) M-C_6-NBD-diacylglycerol standard. (*16*) NBD-amine standard. (*17*) N-Rh-DOPE standard.

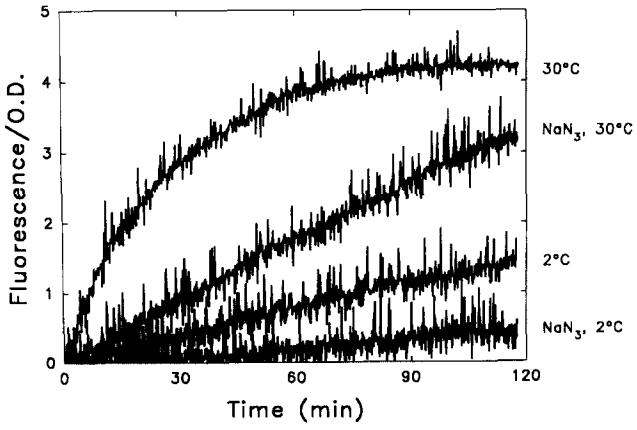

Figure 4. Spectrofluorometric analysis of M-C_6-NBD-PC internalization into CRY3. Internalization assays were performed on the wild-type strain, CRY3. NBD fluorescence was monitored continuously by exciting the fluorophore at 475 nm and monitoring emission at 530 nm. Cell densities were also monitored by reading the OD at 600 nm at regular intervals. Incubation conditions are as shown in the figure.

when vesicles were initially added to an early-log phase cell suspension. Under conditions of continued logarithmic growth, this increase in fluorescence continued for ~30 min, after which it began to plateau. As shown in Table III, the plateau can be explained, at least in part, by degradation of M-C_6-NBD-PC to less fluorescent, aqueous metabolites. When ATP was depleted before incubation at 30°C (trace labeled "NaN_3, 30°C", Fig. 4) the fluorescence increase was reduced significantly (by ~70% at 30 min after the addition of donor vesicles). At 2°C in SDC medium a dramatic decrease was observed in the rate and amount of fluorescence increase; both were inhibited by ~87% at 30 min. Extraction of cellular lipids and separation by TLC showed no degradation of the M-C_6-NBD-PC molecule when incubation was in $SCNaN_3$ medium at 30°C or in SDC at 2°C (Fig. 5). This lack of degradation correlates with the continual increase in cell-associated fluorescence shown in the respective spectrofluorometer traces (Fig. 4). At 2°C with ATP depletion (trace labeled "NaN_3, 2°C," Fig. 4), the fluorescence increase was almost completely blocked (~97%). Presumably, the reduced fluorescence observed in

the spectrofluorometer when cells were incubated at 2°C in SDC medium, or at 30°C with ATP depletion correlates with what is seen in the microscope, namely, continued uptake into the nuclear envelope and mitochondria and elimination of vacuolar uptake (Fig. 2, *A* and *D* and Fig. 3). Similarly, the drastically reduced fluorescence signal in the spectrofluorometer for cells incubated at 2°C with ATP depletion correlates with the blockage of both pathways observed microscopically (Fig. 2 *G*).

Degradation of the Internalized M-C_6-NBD-PC Occurs in the Vacuole

The fate of the internalized phosphatidylcholine was monitored by extracting cells and separating lipids by TLC (Fig. 5). Cells were incubated either at 30°C or at 2°C, under conditions that either maintained or depleted cellular ATP stores. After allowing transport of lipid molecules to occur for 2 h, the cells were extracted with organic solvents, and the aqueous and organic phases were analyzed by TLC. In the Pep+ strain, CRY3, there was significant degradation of M-C_6-NBD-PC only under the condition (30°C, SDC) in which vacuolar fluorescence was seen in the microscope (Fig. 5, lane *9*). Under this condition, four predominant breakdown products appeared in the organic phase. Two of these comigrated with monoacyl-C_6-NBD-phosphatidylcholine and the C_6-NBD-fatty acid markers that were produced by treatment of M-C_6-NBD-PC with phospholipase A_2 (Fig. 5, lane *11*). Another breakdown product comigrated with an M-C_6-NBD-diacylglycerol marker and thus could have been formed by phospholipase C-dependent degradation of M-C_6-NBD-PC molecules (Fig. 5, lane *15*). (The fourth breakdown product occurred under all incubation conditions, and is unidentified at this time.) One predominant (unidentified) breakdown product occurred in the extracted aqueous phase (Table III). Importantly, no significant degradation of M-C_6-NBD-PC occurred when cells were incubated at 2°C or under conditions of ATP depletion (Fig. 5, lanes *6–8*). Together with the microscopic analysis (Figs. 1, 2, and 3), these data argue strongly that metabolism of M-C_6-NBD-PC occurs only in the vacuole.

To examine further the vacuolar location of the phospholipid breakdown, the same extraction protocol was applied to the Pep− strain, CB018. Although the monoacyl-C_6-NBD-phosphatidylcholine and the C_6-NBD-fatty acid metabolites were also present in CB018 (Fig. 5, lane *4*) (consistent with the presence of a phospholipase A_2 activity in the mutant cells), there was a significant difference between the two strains. Although equal numbers of cells were extracted and equal volumes of lipid were spotted onto the TLC plate, there was significantly (~5-fold) more intact M-C_6-NBD-PC present in CB018 than in CRY3 (compare lanes *4* and *9* of Fig. 5). There was a concomitant 7.5-fold reduction in the amount of aqueous break-down product (Table III), consistent with a reduced capacity to metabolize M-C_6-NBD-PC in the Pep− strain. These results also indicated that the site of degradation of M-C_6-NBD-PC was the vacuole.

Quantitation of the fluorescence intensity of the vacuoles observed microscopically by pixel analysis yielded consistent results. In CB018 cells, the average vacuolar pixel brightness was twice that seen for CRY3 (Table III) or for the isogenic Pep+ *MATa* haploid, CRY1 (data not shown). The NBD fluorophore exhibits exquisite sensitivity to the polarity of its environment (Monti et al., 1977). For example, NBD fluorescence is 100 times higher in a phospholipid bilayer than in aqueous environments (Nichols, 1987). Therefore, the fact that degradation of M-C_6-NBD-PC yields products that preferentially partition into the aqueous phase, together with the observation that the vacuoles were twice as bright in CB018 cells as compared to either CRY3 or CRY1 cells, lends further support to the conclusion that less degradation of M-C_6-NBD-PC occurs in Pep− cells.

sec Mutations Block Endocytic Phospholipid Uptake But Not Trafficking to the Nuclear Envelope and Mitochondria

To determine whether there were genetic links between the forward, secretory movement of lipids and the retrograde movement from the plasma membrane demonstrated here, we performed the internalization assay using M-C_6-NBD-PC on yeast strains carrying Ts− mutations in selected secretory (*SEC*) genes (Novick and Schekman, 1979; Novick et al., 1980; Novick et al., 1981). The *SEC* genes can be broadly differentiated as those that are required for the translocation of secretory proteins into the ER, or signal peptide processing in the ER (referred to here as "ER *sec* mutants," exemplified by the *SEC63, SEC65,* and *SEC11* genes) (Bohni et al., 1988; YaDeau et al., 1991; Stirling and Hewitt, 1992; Stirling et al., 1992; Sadler et al., 1989), and those that are required for vesicular transport from the ER to the various secretory organelles (referred to here as "vesicular-transport *sec* mutants," exemplified by the *SEC1, SEC2, SEC4, SEC6, SEC7, SEC12, SEC14, SEC17, SEC18,* and *SEC21* genes) (Novick and Schekman, 1979; Novick et al., 1981; Novick and Schekman, 1983). After internalization assays were performed on these strains, two methods of data analysis were employed. First, the morphology of fluorescence accumulation was documented by creating digital images of representative fields of cells (Fig. 6). Also, by using Image-1/AT image analysis software, the fluorescence intensities of the vacuoles visualized in the digital images of both the Sec+ and Sec− strains were determined. These intensities are expressed as average pixel brightness, and range on an arbitrary scale between 0 and 255.

When the internalization assay was performed on the *sec* mutant strains at a temperature permissive for growth (24°C), both the fluorescence patterns observed in the microscope (Fig. 6) and the pixel brightness of the vacuoles (not shown) were identical to those observed for their isogenic Sec+ strains, and indistinguishable from that observed with CRY3 (Fig. 1) and CB018. However, when the internalization assay was performed at the restrictive temperature (37°C), a functional distinction between the two classes of *sec* mutants was revealed. Mutants that block vesicular transport from the ER through the secretory pathway were also required for lipid endocytosis to the vacuole. These included the secretory-vesicle-accumulating mutants *sec1, sec2, sec4* (a yeast ras-like protein) (Novick and Schekman, 1979; Saminen and Novick, 1987), and *sec6,* which showed almost complete inhibition of lipid flow to the vacuole, although lipid flow to the nuclear-envelope and mitochondria still occurred (Fig. 6, *E–H*). The *sec7* and *sec14* mutants, which affect protein transport out of the Golgi complex (No-

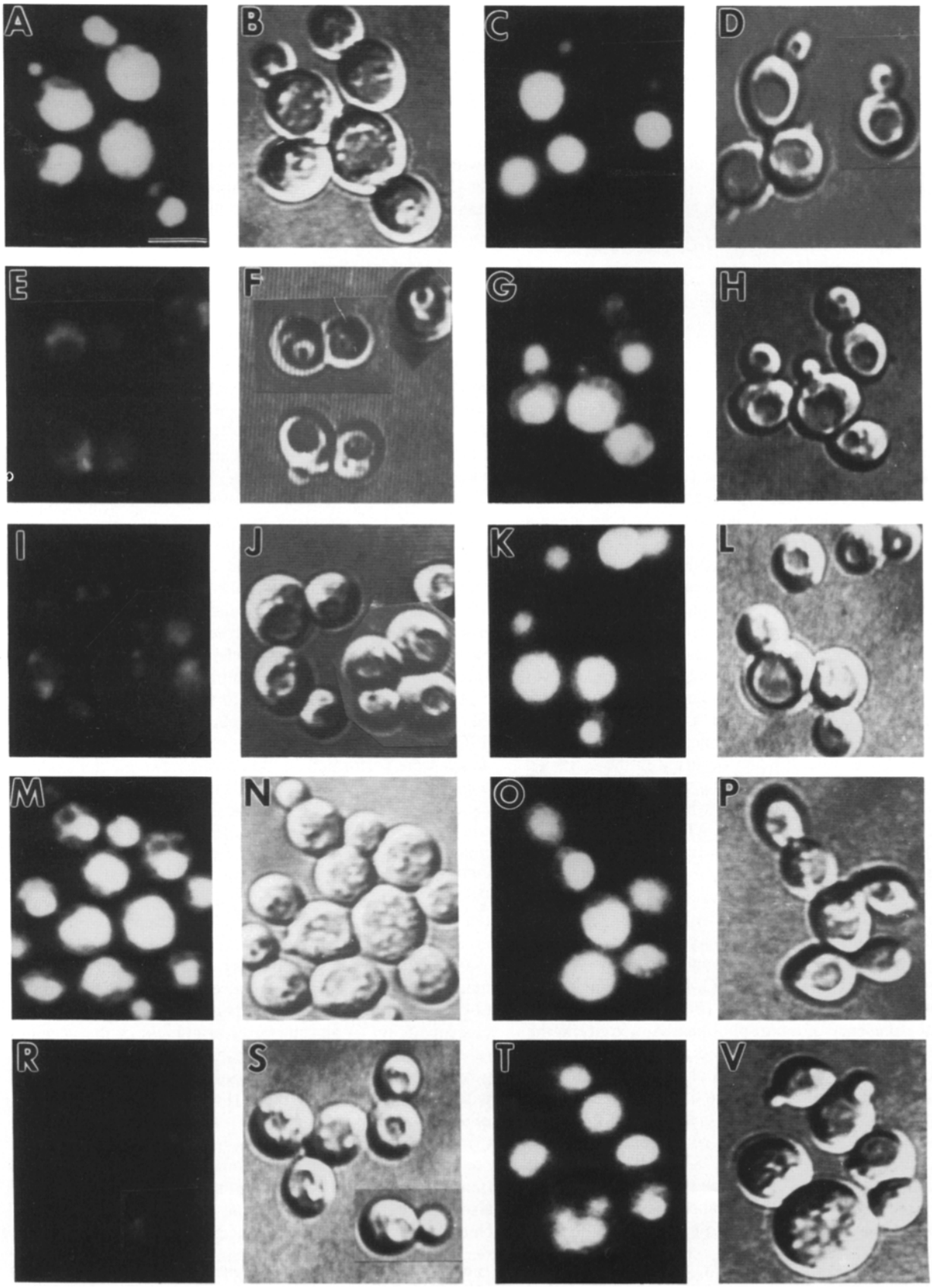

Figure 6. Effect of *sec* mutations on the internalization of M-C_6-NBD-PC. Internalization assays were performed on a variety of wild-type strains and on isogenic strains bearing ts mutations in one of the *SEC* genes. All strains were grown to mid-log phase at 24°C. They were then split, and either shifted to 37°C for 30 min, or kept at 24°C. Internalization assays were then performed, followed by fluorescence microscopy. The panels show: (*A*) CRY1, 37°C, NBD fluorescence (*NBD*). (*B*) CRY1, 37°C, DIC optics (*DIC*). (*C*) CRY1, 25°C, NBD.

vick et al., 1981; Achstetter et al., 1988; Franzusoff and Schekman, 1989; Bankaitis et al., 1990), also blocked internalization to the vacuole (Fig. 6, *I–L*). At the restrictive temperature, Ts− alleles of the *SEC18* gene (which encodes the yeast homolog of the mammalian transport factor NSF [Eakle et al., 1988; Graham and Emr, 1991; Wilson et al., 1989]), of *SEC17* (which encodes the yeast α-SNAP homolog [Clary et al., 1990]), and of *SEC21* (which encodes the yeast homolog of the non-clathrin coat protein, β-COP [Hosobuchi et al., 1992]) reduced phospholipid internalization to the same extent as the late acting *sec* mutants (Fig. 6, *R*, *S*, *T*, and *V*).

The lack of endocytosis in the vesicular-transport *sec* mutant strains can be seen clearly in the digital images in Fig. 6. A statistical analysis of the inhibition of endocytosis is shown in Fig. 7. Because many of the vesicular-transport *sec* mutants had vacuolar pixel brightness values of 0 (their vacuoles were not fluorescent at all), a normal (gaussian) distribution of pixel brightness did not occur, and thus parametric comparison of the means was not possible. For those that had measurable fluorescence, the pixel brightness values ranged widely, but the vast majority did not exceed a value of 20% of the mean of the Sec+ strains. Very few cells from Sec+ strains had vacuoles that were non-fluorescent. The fluorescence intensities for these cells also ranged widely, with mean pixel brightness being ~100. To determine if the distribution of pixel brightness for the Sec− strains was statistically different from the Sec+ strains, a 3 × 2 contingency table was created with bins of 0, >0-20, and >20, and χ^2 analysis was performed. P values were determined, which reflect the statistical significance of the *sec* mutant pixel brightness distributions as compared to their isogenic Sec+ strains. This analysis, shown in Fig. 7, demonstrated that the vacuolar pixel brightness in all of the vesicular-transport *sec* mutants was statistically different from the pixel brightness in the isogenic Sec+ strains to at least the 0.0003 level. Thus, the *SEC* genes that affect membrane traffic during secretion are also required for retrograde lipid traffic during endocytosis. It is possible that the inhibition of endocytic uptake of M-C_6-NBD-PC by the 'vesicular transport' class of *sec* mutants may not be due to direct involvement of each of these gene products in the endocytic pathway. For example, endocytic uptake might be tightly coupled to lipid exocytosis by a regulatory mechanism (see Discussion).

The results with the vesicular transport *sec* mutants sharply contrast those obtained with *sec* mutants that control the translocation of nascent secretory proteins into the ER, or processing in the ER. Mutations in *SEC11* (which encodes a component of the signal peptidase) (Bohni et al., 1988; YaDeau et al., 1991), *SEC63* (a dnaJ homolog) (Sadler et al., 1989), or *SEC65* (which encodes a component of the signal recognition particle) (Stirling and Hewitt, 1992; Stirling et al., 1992), allowed far greater vacuolar accumulation of M-C_6-NBD-PC than did the other *sec* mutants (Fig. 6). In fact, when contingency table statistical analysis was performed on the pixel brightness distributions from these strains, these distributions were found to be not statistically different from the pixel brightness distributions of their isogenic Sec+ alleles (Fig. 7). These strains also differed from the vesicular-transport *sec* mutants in that there was a normal distribution to their pixel brightness values, thus allow-

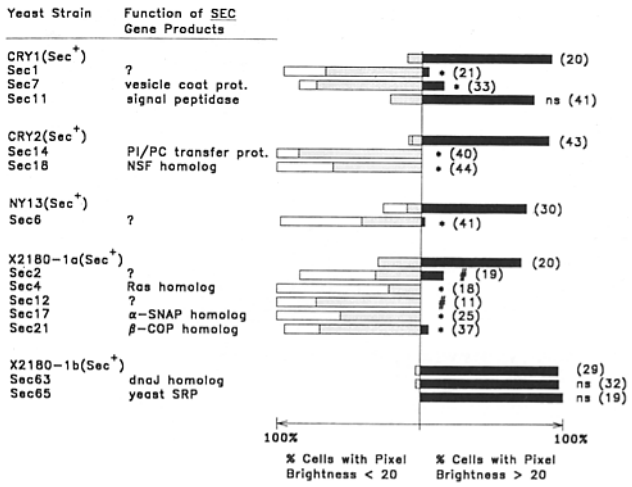

Figure 7. Graphical representation of a 3 × 2 contingency table to test the statistical difference of the distribution of vacuolar pixel brightness values between the *sec* mutant strains and their isogenic Sec+ alleles. 0, >0-20, and >20 are the three pixel brightness ranges that served as statistical bins for the contingency table. The *sec* mutants in this figure are grouped under their respective Sec+ strains. Clear bars represent the % of cells with pixel brightness values of exactly 0. Stippled bars represent the % of cells with pixel brightness values of >0-20. Filled bars represent the % of cells with pixel brightness values of >20. The χ^2 contingency test was used to test whether the pixel brightness distributions of the *sec* strains differed from their isogenic Sec+ alleles. *signifies *sec* strains where $P < 0.0001$. # signifies *sec* strains where $P < 0.0003$. ns signifies *sec* strains whose distributions were not significantly different from their isogenic Sec+ alleles. The number of cells scored is shown in parentheses. Because *sec11*, *sec63*, and *sec65* had no cells with pixel brightness values of 0, 3 × 2 contingency tables could not be made. Instead, 2 × 2 tables were made, and the Fisher's Exact statistical test was performed. With this type of statistical analysis, the pixel brightness distributions for these strains were judged to be not significantly different from their isogenic Sec+ strains. However, unlike the other *sec* mutants, there was a normal distribution of pixel brightness values in the *sec11*, *sec63*, and *sec65* strains. Therefore, the Student's *t* test was performed and is shown in Table IV. Abbreviations used in this figure: *NSF*, NEM-sensitive factor; *PI/PC*, phosphatidylinositol/phosphatidylcholine; *prot*, protein; *SRP*, signal recognition particle.

(*D*) CRY1, 25°C, DIC. The morphology shown for the Sec+ strain, CRY1, is representative of the other Sec+ strains, CRY2, CRY3, NY13, X2180-1A, and X2180-1B. (*E*) *sec1*, 37°C, NBD. (*F*) *sec1*, 37°C, DIC. (*G*) *sec1*, 25°C, NBD. (*H*) *sec1*, 25°C, DIC. The morphology shown for the *SEC1* ts strains is representative of strains that carry ts mutations in the *SEC2*, *SEC4*, and *SEC6* genes. (*I*) *sec7*, 37°C, NBD. (*J*) *sec7*, 37°C, DIC. (*K*) *sec7*, 25°C, NBD. (*L*) *sec7*, 25°C, DIC. The morphology shown for the *SEC7* ts strains is representative of the strain that carries a ts mutation in the *SEC14* gene. (*M*) *sec11*, 37°C, NBD. (*N*) *sec11*, 37°C, DIC. (*O*) *sec11*, 25°C, NBD. (*P*) *sec11*, 25°C, DIC. The morphology shown for the *SEC11* ts strain is representative of the strains that carry ts mutations in the *SEC63* and *SEC65* genes. (*R*) *sec18*, 37°C, NBD. (*S*) *sec18*, 37°C, DIC. (*T*) *sec18*, 25°C, NBD. (*V*) *sec18*, 25°C, DIC. The morphology shown for the *SEC18* ts strain is representative of the strains that carry ts mutations in the *SEC12*, *SEC17*, and *SEC21* genes. Bar, 5 μm.

Table IV. Effect of ER sec mutants and Cycloheximide on Endocytosis of M-C_6-NBD-PC

Strain	Mean vacuolar pixel brightness ± std. dev. (*n. of cells analyzed*)	% Inhibited compared to isogenic Sec$^+$ strain
CRY1	76 ± 34 (20)	–
sec11	34 ± 20 (41)*	55%
X2180-1B	130 ± 73 (29)	–
sec63	79 ± 32 (32)*	39%
sec65	75 ± 34 (19)‡	42%
CRY3	76 ± 20 (42)	–
CRY3 (+cycloheximide)	49 ± 21 (30)*	36%

Internalization assays were performed on the strains as described in Materials and Methods. Vacuolar pixel brightness values were measured using Image1/AT image analysis software. Using the Student's *t* test, the statistical significance of the mean pixel brightness from the *sec* mutants or cycloheximide pretreated cells as compared to the isogenic Sec$^+$ strains was determined. In all cases the two means were significantly different.
* = $p < 0.0006$; ‡ = $p < 0.0035$. A % inhibition was then calculated from the mean vacuolar pixel brightness values.

ing use of the Student's *t* test to determine statistically different means. By this method, the ER *sec* mutants were found to have a modest, but statistically significant affect on lipid endocytosis, inhibiting endocytic lipid flow by 39–55% (Table IV). However, as seen in Fig. 6, even with this level of inhibition, the ER *sec* mutants still carry out substantial lipid endocytosis.

These results suggest that the effects of the *sec* mutations on endocytic phospholipid transport are predominantly due to the inhibition of membrane flow, rather than cargo flow. This interpretation is supported by internalization experiments performed after pretreating cells for 1 h with cycloheximide, a treatment expected to eliminate the newly synthesized protein cargo in transport vesicles, but, at least in the short term, not to eliminate the trafficking of these vesicles along the secretory pathway. When assayed microscopically (data not shown, but comparable to Fig. 6 *M*), cells pretreated with cycloheximide still carried out endocytosis of M-C_6-NBD-PC to a substantial extent, and just as with the ER *sec* mutants, deposited the fluorescent phospholipid into the vacuole. Pixel brightness analysis of vacuoles (Table IV) revealed that in cycloheximide-treated cells lipid endocytosis was affected to much the same degree as with the ER *sec* mutants, being inhibited by ~36% as compared to cells that were left untreated.

Although the endocytic pathway was dependent on many *SEC* genes, it was not dependent on a functional clathrin heavy chain. Thus, in the strain GPY184, having a Ts– clathrin heavy chain gene (*chcl-52*), endocytic lipid traffic continued even after incubation of these cells for 1.5 h at the restrictive temperature (Table V). This was in sharp contrast to the rapid effects seen in this strain (within 15 min) on proper retention of Golgi-resident enzymes and maturation of pro-CPY (Seeger and Payne, 1992*a*,*b*).

Although none of the other 12 *sec* mutants tested had any inhibitory effect on the non-endocytic transport of M-C_6-NBD-PC to the nuclear envelope and mitochondria, we did observe a reproducible inhibition of this traffic in *secl8* cells (Fig. 6 *R*). Although a comparison of pixel brightness values showed that this inhibition was less that the *secl8*-mediated inhibition of endocytic lipid flow (~55% compared to ~98%), a requirement for the *secl8* gene product in non-endocytic lipid traffic is suggested by this data.

The *sec* mutant experiments provide further evidence that two distinct pathways exist for retrograde lipid traffic, because whereas lipid flow to the vacuole was blocked by many *sec* mutations, with the exception of *secl8*, lipid flow to the nuclear envelope and mitochondria was not. However, although non-endocytic lipid traffic was largely independent of *SEC* genes, it did appear to be protein-mediated, due to its inhibition by the two (chemically distinct) sulfhydryl reagents, NEM, and pCMBS (Table VI). It was inhibited by 89% when cells were pretreated with 2 mM NEM, by 40% when pretreatment was with 10 mM pCMBS, and by 50% when pretreatment was with 50 mM pCMBS.

Discussion

Two Pathways of Lipid Flow Occur during the Internalization of M-C_6-NBD-PC

The data presented here have provided evidence for two previously undocumented lipid transport pathways in yeast (Fig. 8). First, plasma membrane phospholipids can be actively internalized by an endocytic mechanism, concentrated and degraded in the vacuole (Fig. 8 *A*). A second pathway, which is largely independent of *SEC* gene function, deposits plasma membrane phospholipids in the nuclear envelope and mitochondria (Fig. 8 *B*). This pathway resembles the non-endocytic phospholipid flip-flow pathways that have been observed in mammalian systems.

The two pathways shown in Fig. 8 share a common first step: insertion of the M-C_6-NBD-PC molecules into the yeast plasma membrane. The yeast plasma membrane appears to have a lower affinity for NBD-labeled phospholipids than do the plasma membranes of mammalian cells. "Ring

Table V. Effect of a Clathrin Heavy Chain ts Allele on Endocytosis of M-C_6-NBD-PC

Strain	Relevant phenotype	Mean vacuolar pixel brightness ± std. dev. (*n. of cells analyzed*)
GPY55-15B	CHC1 (wt)	77 ± 55 (40)
GPY184	chc1 (ts)	66 ± 50 (34)*

Internalization assays were performed on the two strains as described in Materials and Methods. Vacuolar pixel brightness values were measured using Image1/AT image analysis software.
* The mean vacuolar pixel brightness for the wt and ts CHC1 alleles were analyzed using the Student's *t* test, and were found to be not statistically different from one another ($p < 0.37$).

Table VI. Effect of NEM and pCMBS on the Internalization of M-C_6-NBD-PC to the Nuclear Envelope at 2°C

Strain	Nuclear envelope pixel brightness ± std. dev. (*n. of cells analyzed*)	% Inhibition
CRY3	5.8 ± 1.2 (23)	–
CRY3 (pretreated with 2 mM NEM	0.65 ± 0.29 (34)*	89%
CRY3	7.33 ± 1.67 (18)	–
CRY3 (pretreated with 10 mM pCMBS)	4.20 ± 1.38 (28)*	42%
CRY3	10.88 ± 4.66 (17)	–
CRY3 (pretreated with 50 mM pCMBS)	5.51 ± 5.32 (14)‡	50%

Cells were either pretreated for 30 min with 2 mM NEM, 10 mM pCMBS, 50 mM pCMBS (as described in Materials and Methods), or left untreated. Internalization assays were then performed at 2°C, and the fluorescence in the nuclear envelope was determined as an average pixel brightness value using Image1/AT image analysis software. The Student's *t* test was used to determine the statistical significance of the mean pixel brightness from treated or untreated cells. The two means were statistically different from each other. * = $p < 0.0001$, ‡ = $p < 0.0056$. A % inhibition by NEM or pCMBS was then determined from the mean pixel brightness values.

staining" of the plasma membrane, typical in mammalian cells (Struck and Pagano, 1980), was never seen with yeast cells, even when incubated under conditions that inhibited phospholipid internalization (Fig. 2 *G*). Two lines of evidence support the hypothesis that the reduced level of phospholipid insertion was due to a lowered capacity of the yeast plasma membrane (as compared to mammalian plasma membranes) for exogenous lipids, and not to a lowered rate by which these lipids could diffuse through the yeast cell wall and insert into the plasma membrane. First, enzymatic removal of the cell wall with zymolyase (β-1,3-glucanase) did not increase plasma membrane fluorescence (data not shown). Second, as shown in Fig. 2, if either the rate of diffusion through the cell wall or the rate of insertion of lipids into the plasma membrane were rate limiting, then inhibition of lipid flux by incubation in sodium azide should have resulted in substantial accumulation of the fluorescent phospholipid in the plasma membrane, which was not observed. Thus, the labeling of the plasma membrane must be limited by its capacity for exogenous phospholipids, not on their rate of insertion. This low level of insertion indicates that the partition coefficient for M-C_6-NBD-PC into the yeast plasma membrane is significantly lower than for the artificial vesicles used as donors in these experiments (Nichols, 1985). The partition coefficient of the yeast plasma membrane for NBD-labeled phospholipids may be reduced relative to the donor vesicles by the presence of sterols (i.e., ergosterol) (Phillips et al., 1987) or other lipid components of the mem-

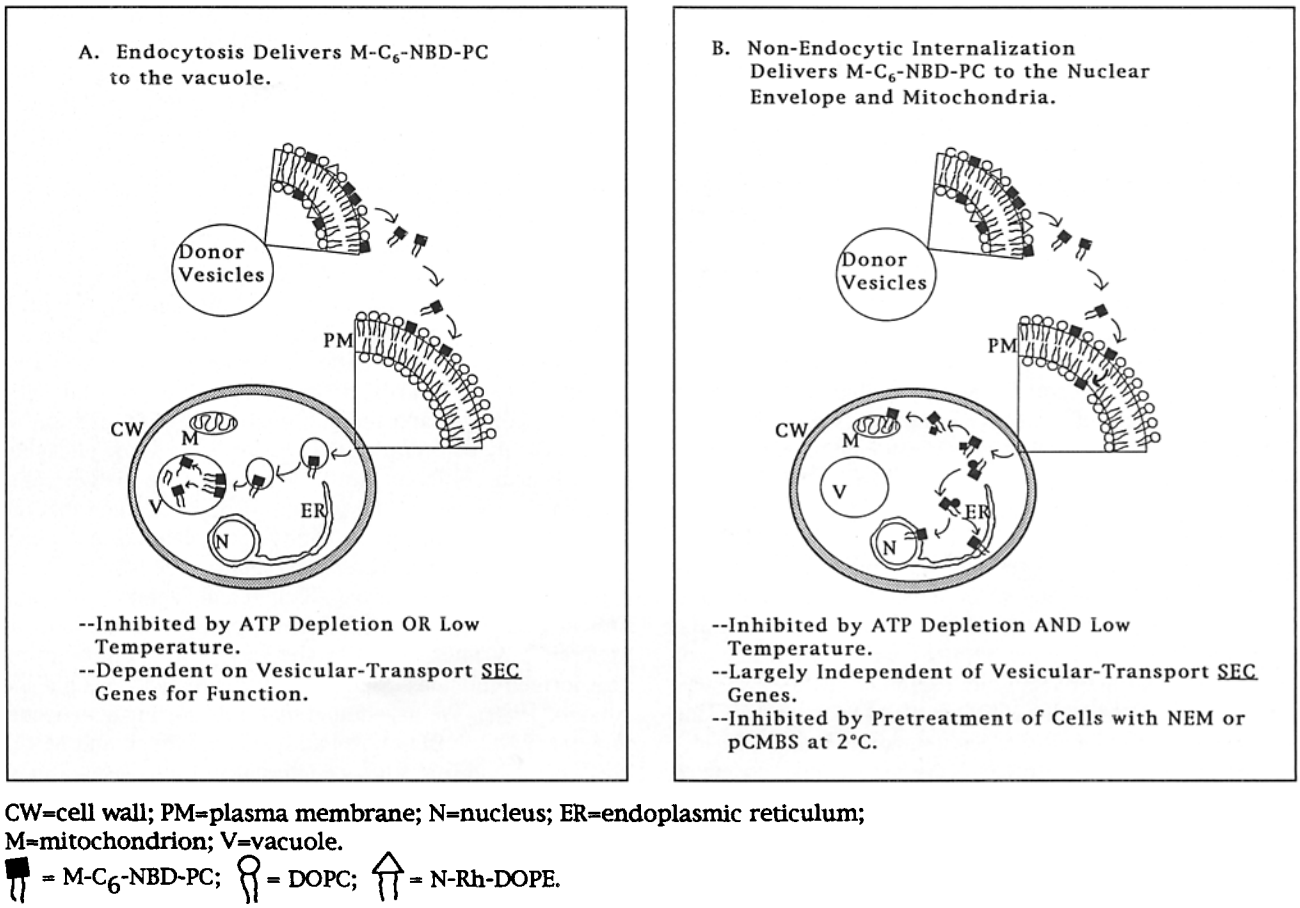

Figure 8. Working model of the two internalization pathways for M-C_6-NBD-PC into yeast cells.

brane, the unusually high turgor pressure of the yeast plasma membrane (Gustin et al., 1988) or by constraints imposed by cytoskeletal elements (Chowdhury et al., 1992) that limit membrane expansion required for lipid insertion. Recent investigations into the fluidity of the yeast plasma membrane employing FRAP indicate that the lateral mobility of lipids in the yeast membrane is significantly lower than that observed in mammalian cells (Greenberg and Axelrod, 1993). The constraints responsible for this reduced lateral mobility are also likely to reduce the extent to which exogenous phospholipids can be inserted into the plasma membrane.

Retrograde transport of NBD-labeled phospholipids into cultured mammalian cells is usually monitored after the removal of exogenous donor vesicles after preloading the plasma membrane with the fluorescent phospholipid (Sleight and Pagano, 1984). In contrast, the low level of M-C_6-NBD-PC insertion into the yeast plasma membrane required continual incubation in the presence of vesicles to accumulate measurable levels of intracellular fluorescence. Control experiments (Table II) confirmed that, even in the constant presence of donor vesicles, internalization occurred only after M-C_6-NBD-PC monomers dissociated from these vesicles and inserted into the plasma membrane. Additionally, because cell-associated fluorescence increased only as a result of lipid-internalization, we could estimate the relative rates of the two internalization pathways by monitoring cell-associated fluorescence continuously in the spectrofluorometer (Fig. 4).

Under normal growth conditions, the majority (~70%) of M-C_6-NBD-PC molecules were internalized by endocytosis, and were transported to the vacuole (Fig. 8 *A*). The vacuolar pathway has been termed "endocytic" for three reasons. First, low temperatures and decreased cellular ATP levels, two classical conditions in which endocytosis is inhibited (Anderson et al., 1977; Draper and Simon, 1980; Helenius et al., 1980), both completely inhibited transport of M-C_6-NBD-PC to the vacuole. Second, a number of ts *sec* mutations (that are known to inhibit the vesicular traffic involved in protein secretion at the restrictive temperature) also blocked transport of M-C_6-NBD-PC to the vacuole. This implies that transport to the vacuole may require membrane-enclosed structures, either endocytic vesicles or possibly tubules. Third, the target organelle of this traffic, the vacuole (yeast lysosome), is the terminal destination for endocytic transport of a variety of markers (Riezman, 1985; Raths et al., 1993), and thus provides a landmark for endocytic traffic in yeast. Endocytosis of M-C_6-NBD-PC does not appear to be clathrin-dependent (Table V). In addition, recent experiments (Kean, L. S., R. S. Fuller, J. W. Nichols, unpublished results) suggest that endocytosis of M-C_6-NBD-PC is also independent of selected Vacuolar Protein Sorting (*VPS*) genes (Banta et al., 1988; Rothman et al., 1989) and the END genes required for internalization of pheromones and their receptors (Raths et al., 1993).

The second pathway lacks hallmarks of endocytosis. This pathway (1) is less sensitive to low temperature and ATP levels than the endocytic pathway, (2) is largely independent of *SEC* gene function, and (3) results in the delivery of M-C_6-NBD-PC to the mitochondria and nuclear envelope, rather than to the vacuole. Although our results clearly show that the vacuole is excluded from non-endocytic traffic (Figs. 2 and 3), we cannot rule out some labeling of other organelles such as the ER and Golgi, in part due to the lack of appropriate vital markers for these two organelles. In fact, since the ER and nuclear envelope are connected in yeast, it is possible that M-C_6-NBD-PC is deposited in this organelle as well. However, we have found that M-C_6-NBD-phosphatidylethanolamine labels an extensive reticular network, most likely the ER, via a non-endocytic route (Kean, L. S., R. S. Fuller, J. W. Nichols, unpublished results). This suggests that the level of M-C_6-NBD-PC in the ER is low.

The non-endocytic pathway is inhibited by the sulfhydryl reagents NEM and pCMBS, and thus appears to be protein-mediated. While NEM has been shown to be membrane-permeant at 37°C (Abbot and Schacter, 1976; May, 1985; D'Amore and Lo, 1986), pCMBS has been shown to be membrane impermeant in a variety of cell systems (Rothstein, 1970; May, 1985; D'Amore and Lo, 1986). While both reagents inhibit the non-endocytic pathway at 2°C (Table VI), NEM inhibition (89%) is more extensive than pCMBS inhibition (40–50%). Two possible explanations exist for the greater inhibition by NEM. NEM may simply modify (and inhibit) a cell-surface protein more effectively than pCMBS, and thereby lead to greater inhibition of the non-endocytic pathway. Alternatively, NEM may also modify intracellular proteins which are important for specific traffic to the nuclear envelope and mitochondria. Inhibition of these intracellular proteins might further shut down the flux of M-C_6-NBD-PC and therefore lead to a more complete reduction in the intracellular fluorescence accumulation.

The non-endocytic trafficking of M-C_6-NBD-PC to the nuclear envelope and mitochondria in yeast resembles the non-endocytic trafficking of NBD-phosphatidylethanolamine and NBD-phosphatidylserine in untransformed mammalian cell lines (Martin and Pagano, 1987; Sleight and Pagano, 1985), and of NBD-phosphatidylcholine in virally transformed human lung fibroblasts (Sleight and Abanto, 1989) which has been shown to occur by protein-mediated flip-flop (Martin and Pagano, 1987; Sleight and Pagano, 1985; Sleight and Abanto, 1989). Inhibition of this putative yeast flip-flop activity by NEM suggests that it may be more closely related to the aminophospholipid flip-flop activities than to the NEM-resistant phosphatidylcholine flip-flop activity found in virally transformed human lung fibroblasts. An additional similarity between the yeast non-endocytic transport pathway and the mammalian flip-flop pathway is the selectivity that these pathways display towards phospholipids bearing different head-groups. In mammalian cells, lipid sorting occurs at the plasma membrane, such that the aminophospholipids (phosphatidylethanolamine and phosphatidylserine) are preferentially internalized by the non-endocytic (flip-flop) pathway (Sleight and Pagano, 1985; and Martin and Pagano, 1987), while phosphatidylcholine is preferentially internalized by the endocytic pathway in untransformed cell lines (Sleight and Pagano, 1984; Sleight and Abanto, 1989). We have found that lipid sorting also occurs in yeast. M-C_6-NBD-phosphatidylethanolamine and M-C_6-NBD-phosphatidylserine are internalized into yeast almost exclusively via the non-endocytic pathway, and are trafficked by this pathway to the ER, nuclear envelope and mitochondria, but not to the vacuole (Kean, L. S., R. S. Fuller, and J. W. Nichols, unpublished results). This is in striking con-

trast to results shown here with M-C_6-NBD-PC (Fig. 1) in which trafficking occurs predominantly by endocytosis to the vacuole.

It is interesting that only one *sec* mutant, *sec18*, appeared to have any substantial effect on the non-endocytic internalization pathway (Fig. 6 *R*). *SEC18* is also the only *SEC* gene that has been shown to be required in all steps of vesicular traffic in yeast (Graham and Emr, 1991), being required for fusion of vesicles with target membranes on all organelles that have been tested. It is possible that a fusion reaction is also required during the non-endocytic targeting of lipids, and that *SEC18* plays a role in this process.

Flip-flop activities have been observed in the membranes of many cell systems, and have been implicated in maintaining lipid asymmetry across the membrane bilayers (Rousselet et al., 1976; van Meer and Op den Kamp, 1982). Asymmetry generated by the combined action of flip-flop proteins and phospholipid transfer proteins could play a role in differentiating organelles, or in targeting proteins to subdomains of a continuous lipid bilayer. The selective transport of M-C_6-NBD-PC to the nuclear envelope and mitochondrial membranes by the non-endocytic route suggests the existence of specific intracellular transport pathways, perhaps relying on specific lipid transfer proteins. The phosphatidylinositol-phosphatidylcholine transfer protein encoded by the *SEC14* gene would not be implicated in these transfer reactions (at least for the transfer of M-C_6-NBD-PC), since non-endocytic phospholipid transport is not blocked in a *sec14* ts mutant assayed at the non-permissive temperature.

Despite the proposed importance of lipid flip-flop proteins for a variety of membrane traffic events, the proteins responsible for transbilayer lipid movement remain to be identified. Having an assay for flip-flop in yeast should assist the identification of this class of proteins, and the genes that encode them.

Two Models to Explain the Link between Secretion and Lipid Endocytosis

As is shown in Figs. 6 and 7 and Table IV, the *SEC* genes required for proper membrane flow during secretion were also required for lipid endocytosis. These vesicular-transport *SEC* genes were distinguished from genes such as *SEC63*, *SEC65*, and *SEC11*, which are required very early in the secretory pathway for translocation of proteins into and processing in the ER, and were not required for endocytic lipid traffic. Two distinct models can account for the striking interconnection that we have noticed between endocytic lipid transport and vesicular-transport *SEC* gene function.

One model states that the *SEC* gene products required for vesicular transport are also directly and functionally required for endocytic events. Given the large number of *sec* mutants that also inhibit lipid endocytosis, this model predicts that the biochemical links between endocytosis and secretion must be extensive. The second model assumes no direct requirement for *SEC* gene products in the mechanism of lipid internalization, but rather, a regulatory coupling of the two pathways. Exocytic trafficking might require retrograde transport of excess phospholipid from the plasma membrane back to intracellular organelles. Analogous retrograde vesicular transport pathways have been hypothesized both on theoretical (Rothman, 1981) and experimental grounds (Lippincott-Schwartz et al., 1989; Dean and Pelham, 1990; Hsu et al., 1991). Indirect evidence for such a process in yeast is found in the analysis of inositol auxotrophs (*inol* mutants) under conditions of inositol starvation. Such cells exhibit a rapid cessation of membrane growth, but secretion appears to continue unabated (Henry et al., 1977; Atkinson and Ramirez, 1984). Thus, retrograde transport of lipids delivered to the plasma membrane by secretory vesicle fusion could complete a "closed cycle" of lipid transport, effectively coupling exocytosis and lipid endocytosis. Consistent with this model, preliminary quantitative measurements of the rate of internalization of M-C_6-NBD-PC by the endocytic pathway suggest that significantly more than one plasma membrane-equivalent is internalized per cell division cycle (Kean, L. S., R. S. Fuller, and J. W. Nichols, unpublished data). Thus, instead of there being a specific requirement for the individual proteins encoded by the various *SEC* genes, there could be a regulatory coupling of the two processes to ensure plasma membrane homeostasis. In effect, failure in either process would generate an inhibitory signal that would shut off the other process. A key question raised by the regulatory coupling of the two processes is how signaling between the two pathways occurs. One possibility might be that a mechanism exists that measures the flux of exocytic membrane traffic directly and communicates this information to the endocytic apparatus. A second possibility is that there is a system capable of sensing changes in the physical state of the plasma membrane that occur upon a reduction of the rate of exocytosis (Gustin et al., 1988; Martinac et al., 1990; Brewster et al., 1993).

The data presented in this paper do not distinguish between the two models for explaining the linkage of endo- and exo-cytosis. However, the isolation of single mutations that affect lipid exocytosis or lipid endocytosis exclusively would be incompatible with the regulatory coupling hypothesis.

The authors wish to thank Donald Wigston for valuable discussions and instruction on fluorescence microscopy techniques, and Marla Luskin and Donald Wigston for use of the fluorescence microscope. The authors also thank Greg Payne, Kevin Redding, Howard Riezman, and Randy Schekman for providing strains for helpful discussions.

This work was supported in part by a National Institutes of Health grant (GM39697) and a Lucille P. Markey Scholar Award (87-91) to R. S. Fuller and by grant #BE-68054 from the American Cancer Society to J. W. Nichols. L. S. Kean is a recipient of a Howard Hughes Medical Institute Predoctoral Fellowship.

Received for publication 12 May 1993 and in revised form 22 September 1993.

References

Abbot, R. E., and D. Schacter. 1976. Impermeant maleimides: oriented probes of erythrocyte membrane proteins. *J. Biol. Chem.* 251:7176–7183.

Ames, B. N., and D. T. Dubin. 1960. The role of polyamines in the neutralization of bacteriophage deoxyribonucleic acid. *J. Biol. Chem.* 235:769–775.

Anderson, R. G. W., M. S. Brown, and J. L. Goldstein. 1977. Role of the coated endocytic vesicle in the uptake of receptor-bound low density lipoprotein in human fibroblasts. *Cell.* 10:351–364.

Achstetter, T., A. Franzusoff, C. Field, and R. Schekman. 1988. *SEC7* encodes an unusual high molecular weight protein required for membrane traffic from the yeast Golgi apparatus. *J. Biol. Chem.* 263:11711–11717.

Atkinson, K. D., and R. M. Ramirez. 1984. Secretion can proceed uncoupled from net plasma membrane expansion in inositol-starved Saccharomyces cerevisiae. *J. Bact.* 160:80–86.

Bankaitis, V. A., F. R. Aitken, A. E. Cleves, and W. Dowhan. 1990. An essential role for a phospholipid transfer protein in yeast Golgi function. *Nature (Lond.).* 347:561–562.

Banta, L. M., J. S. Robinson, D. J. Klionsky, and S. D. Emr. 1988. Organelle assembly in yeast: characterization of yeast mutants defective in vacuolar biogenesis and protein sorting. *J. Cell Biol.* 107:1369–1383.

Bishop, W. R., and R. M. Bell. 1988. Assembly of phospholipids into cellular membranes: biosynthesis, transmembrane movement and intracellular translocation. *Annu. Rev. Cell Biol.* 4:579–610.

Bohni, P. C., R. J. Deshaies, and R. W. Schekman. 1988. *SEC11* is required for signal peptide processing and yeast cell growth. *J. Cell Biol.* 106: 1035–1042.

Brewster, J. L., T. de Valoir, N. D. Dwyer, E. Winter, and M. C. Gustin. 1993. An osmosensing signal transduction pathway in yeast. *Science (Wash. DC).* 259:1760–1763.

Chowdhury, S., K. W. Smith, and M. C. Gustin. 1992. Osmotic stress and the yeast cytoskeleton: phenotype-specific suppression of an actin mutation. *J. Cell Biol.* 118:561–571.

Clary, D. O., I. C. Griff, and J. E. Rothman. 1990. SNAPs, a family of NSF attachment proteins involved in intracellular membrane fusion in animals and yeast. *Cell.* 61:709–721.

D'Amore, T., and T. C. Y. Lo. 1986. Hexose transport in L6 rat myoblasts. II. The effects of sulfhydryl reagents. *J. Cell Physiol.* 127:106–113.

Dean, N., and H. R. B. Pelham. 1990. Recycling of proteins from the Golgi compartments to the ER in yeast. *J. Cell Biol.* 111:369–377.

Draper, R. K., and M. I. Simon. 1980. The entry of diphtheria toxin into the mammalian cell cytoplasm: evidence for lysosomal involvement. *J. Cell Biol.* 87:849–854.

Eakle, K. A., M. Bernstein, and S. D. Emr. 1988. Characterization of a component of the yeast secretion machinery: identification of the SEC18 gene product. *Mol. Cell Biol.* 8:4098–4109.

Franzusoff, A., and R. Schekman. 1989. Functional compartments of the yeast golgi apparatus are defined by the *sec7* mutation. *EMBO (Eur. Mol. Biol. Organ.) J.* 8:2695–2702.

Franzusoff, A., E. Lauze, and K. E. Howell. 1992. Immuno-isolation of Sec7p-coated transport vesicles from the yeast secretory pathway. *Nature (Lond.).* 355:173–175.

Graham, T. R., and S. D. Emr. 1991. Compartmental organization of Golgi-specific protein modification and vacuolar protein sorting events defined in a yeast *sec18* (NSF) mutant. *J. Cell Biol.* 114:207–218.

Greenberg, M. L., and D. Axelrod. 1993. Slow lateral diffusion of lipid probes in yeast cell membranes. *Biophys. J.* 64:A123.

Gustin, M. C., X. L. Zhou, B. Martinac, and C. Kung. 1988. A mechanosensitive ion channel in the yeast plasma membrane. *Science (Wash. DC).* 242:762–765.

Helenius, A., M. Marsh, and J. White. 1980. The entry of viruses into animal cells. *Trends Biochem. Sci.* 5:104–106.

Henry, S. A., K. D. Atkinson, A. I. Kolat, and M. R. Culbertson. 1977. Growth and metabolism of inositol-starved *Saccharomyces cerevisiae. J. Bacteriol.* 130:472–484.

Hjelmstad, R., and R. Bell. 1987. Mutants of Saccharomyces cerevisiae defective in sn-1,2-diacylglycerol cholinephosphotransferase. Isolation, characterization and cloning of the CPT1 gene. *J. Biol. Chem.* 262:3909–3917.

Hosobuchi, M., T. Kreis, and R. Schekman. 1992. *SEC21* is a gene required for ER to Golgi protein transport that encodes a subunit of a yeast coatomer. *Nature (Lond.).* 360:603–605.

Hsu, V. W., L. C. Yuan, J. G. Nuchtern, J. Lipincott-Schwartz, J. Hannelin, and R. D. Klausner. 1991. A recycling pathway between the endoplasmic reticulum and the Golgi apparatus for retention of unassembled MHC class I molecules. *Nature (Lond.).* 352:441–444.

Jones, E. W. 1991. Three proteolytic systems in the yeast *Saccharomyces cerevisiae. J. Biol. Chem.* 266:7963–7966.

Koval, M., and R. E. Pagano. 1990. Sorting of an internalized plasma membrane lipid between recycling and degradative pathways in normal and Niemann-Pick, type A fibroblasts. *J. Cell Biol.* 111:429–442.

Lippincott-Schwartz, J., L. C. Yuan, J. S. Bonifacino, and R. D. Klausner. 1989. Rapid redistribution of Golgi proteins into the ER in cells treated with Brefeldin A: evidence for membrane cycling from Golgi to ER. *Cell.* 56:801–813.

Martin, O. C., and R. E. Pagano. 1987. Transbilayer movement of fluorescent analogs of phosphatidylserine and phosphatidylethanolamine at the plasma membrane of cultured cells. *J. Biol. Chem.* 262:5890–5898.

Martinac, B., J. Adler, and C. Kung. 1990. Mechanosensitive ion channels of E. coli activated by amphipaths. *Nature (Lond.).* 348:261–263.

May, J. M. 1985. The inhibition of hexose transport by permeant and impermeant sulfhydryl agents in rat adipocytes. *J. Biol. Chem.* 260:462–467.

Monti, J. A., S. T. Christian, W. A. Shaw, and W. H. Finley. 1977. Synthesis and properties of a fluorescent derivative of phosphatidylcholine. *Life Sci.* 21:345–356.

Nichols, J. W. 1985. Thermodynamics and kinetics of phospholipid monomer-vesicle interaction. *Biochemistry.* 24:6390–6398.

Nichols, J. W. 1987. Binding of fluorescent-labeled phosphatidylcholine to rat liver nonspecific lipid transfer protein. *J. Biol. Chem.* 262:14172–14177.

Nichols, J. W., and R. E. Pagano. 1983. Resonance energy transfer assay of protein-mediated lipid transfer between vesicles. *J. Biol. Chem.* 258: 5368–5371.

Novick, P., and R. Schekman. 1979. Secretion and cell-surface growth are blocked in a temperature-sensitive mutant of *Saccharomyces cerevisiae. Proc. Natl. Acad. Sci. USA.* 76:1858–1862.

Novick, P., and R. Schekman. 1983. Export of major cell surface proteins is blocked in yeast secretory mutants. *J. Cell Biol.* 96:541–547.

Novick, P., S. Ferro, and R. Schekman. 1981. Order of events in the yeast secretory pathway. *Cell.* 25:461–469.

Novick, P., C. Field, and R. Schekman. 1980. Identification of 23 complementation groups required for post-translational events in the yeast secretory pathway. *Cell.* 21:205–215.

Pagano, R. E. 1990*a*. Lipid traffic in eukaryotic cells: mechanisms for intracellular transport and organelle-specific enrichment of lipids. *Curr. Opin. Cell Biol.* 2:652–663.

Pagano, R. E. 1990*b*. The Golgi apparatus: insights from lipid biochemistry. *Biochem. Soc. Trans.* 18:361–366.

Pagano, R. E., and R. G. Sleight. 1985. Defining lipid transport pathways in animal cells. *Science (Wash. DC).* 229:1051–1057.

Phillips, M. C., W. J. Johnson, and G. H. Rothblat. 1987. Mechanisms and consequences of cellular cholesterol exchange and transfer. *Biochim. Biophys. Acta.* 906:223–276.

Raths, S., J. Rohrer, F. Crausaz, and H. Reizman. 1993. *end3* and *end4*: two mutants defective in receptor-mediated and fluid-phase endocytosis in S. cerevisiae. *J. Cell Biol.* 120:55–65.

Riezman, H. 1985. Endocytosis in yeast: several of the yeast secretory mutants are defective in endocytosis. *Cell.* 40:1001–1009.

Rothman, J. E. 1981. The Golgi apparatus: two organelles in tandem. *Science (Wash. DC).* 213:1212–1219.

Rothman, J. H., I. Howald, and T. H. Stevens. 1989. Characterization of genes required for protein sorting and vacuolar function in the yeast *Saccharomyces cerevisiae. EMBO (Eur. Mol. Biol. Organ.) J.* 8:2057–2065.

Rothstein, A. 1970. Sulfhydryl groups in membrane structure and function. *Curr. Top. Membr. Transp.* 1:135–176.

Rousselet, A., C. Guthman, J. Matricon, A. Bienvenue, and J. P. F. Devaux. 1976. Study of the transverse diffusion of spin labeled phospholipids in biological membranes. I. Human red blood cells. *Biochim. Biophys. Acta.* 426:357–371.

Sadler, I., A. Chiang, T. Kurihan, J. Rothblatt, J. Woy, and P. Silver. 1989. A yeast gene important for protein assembly into the endoplasmic reticulum and the nucleus has homology to DnaJ, an Escherichia coli heat shock protein. *J. Cell Biol.* 109:2665–2675.

Saminen, A., and P. J. Novick. 1987. A ras-like protein is required for a post-Golgi event in yeast secretion. *Cell.* 49:527–538.

Schroit, A. J., and R. F. A. Zwaal. 1991. Transbilayer movement of phospholipids in red cell and platelet membranes. *Biochim. Biophys. Acta.* 1071: 313–329.

Seeger, M., and G. S. Payne. 1992*a*. Selective and immediate effects of clathrin heavy chain mutations on Golgi membrane protein retention in Saccharomyces cerevisiae. *J. Cell Biol.* 118:531–540.

Seeger, M., and G. S. Payne. 1992*b*. A role for clathrin in the sorting of vacuolar proteins in the Golgi complex of yeast. *EMBO (Eur. Mol. Biol. Organ.) J.* 11:2811–2818.

Sherman, F., G. R. Fink, and J. B. Hicks. 1986. Methods in Yeast Genetics. Cold Spring Harbor Laboratory Press, Cold Spring Harbor, NY. 164–165.

Sleight, R. G., and R. E. Pagano. 1983. Rapid appearance of newly synthesized phosphatidylethanolamine at the plasma membrane. *J. Biol. Chem.* 258:9050–9058.

Sleight, R. G., and R. E. Pagano. 1984. Transport of a fluorescent phosphatidylcholine analog from the plasma membrane to the Golgi apparatus. *J. Cell Biol.* 99:742–751.

Sleight, R. G., and R. E. Pagano. 1985. Transbilayer movement of a fluorescent phosphatidylethanolamine analogue across the plasma membranes of cultured mammalian cells. *J. Biol. Chem.* 260:1146–1154.

Sleight, R. G., and M. N. Abanto. 1989. Differences in intracellular transport of a fluorescent phosphatidylcholine analog in established cell lines. *J. Cell Sci.* 93:363–374.

Stevens, T., B. Esmon, and R. Schekman. 1982. Early stages in the yeast secretory pathway are required for transport of carboxypeptidase Y to the vacuole. *Cell.* 30:439–448.

Stirling, C. J., and E. W. Hewitt. 1992. The *S. cerevisiae* SEC65 gene encodes a component of yeast signal recognition particle with homology to human SRP19. *Nature (Lond.).* 356:534–537.

Stirling, C. J., J. Rothblatt, M. Hosobuchi, R. Deshaies, and R. Schekman. 1992. Protein translocation mutants defective in the insertion of integral membrane proteins into the endoplasmic reticulum. *Mol. Biol. Cell.* 3:129–142.

Struck, D. K., and R. E. Pagano. 1980. Insertion of fluorescent phospholipids into the plasma membrane of a mammalian cell. *J. Biol. Chem.* 255: 5404–5410.

Struck, D. K., D. Hoekstra, and R. E. Pagano. 1981. Use of resonance energy transfer to monitor membrane fusion. *Biochemistry.* 20:4093–4099.

Takeshige, K., M. Baba, S. Tsuboi, T. Noda, and Y. Ohsumi. 1992. Autophagy in yeast demonstrated with proteinase-deficient mutants and conditions for its induction. *J. Cell Biol.* 119:301–311.

Urbani, I., and R. D. Simoni. 1990. Cholesterol and vesicular stomatitis virus

G protein take separate routes from the endoplasmic reticulum to the plasma membrane. *J. Biol. Chem.* 265:1919–1923.

van Meer, G. 1989. Lipid traffic in animal cells. *Annu. Rev. Cell Biol.* 5:247–275.

van Meer, G., and J. A. F. Op den Kamp. 1982. Transbilayer movement of various phosphatidylcholine species in intact human erythrocytes. *J. Cell. Biochem.* 19:193–204.

Weisman, L. S., R. Bacallao, and W. Wickner. 1987. Multiple methods of visualizing the yeast vacuole permit evaluation of its morphology and inheritance during the cell cycle. *J. Cell Biol.* 105:1539–1547.

Wilson, D. W., C. A. Wilcox, G. C. Flynn, E. Chen, W.-J. Kuang, W. J. Henzel, M. R. Block, A. Ullrich, and J. E. Rothman. 1989. A fusion protein required for vesicle-mediated transport in both mammalian cells and yeast. *Nature (Lond.).* 339:355–359.

YaDeau, J. T., C. Klein, and G. Blobel. 1991. Yeast signal peptidase contains a glycoprotein and the Sec11 gene product. *Proc. Natl. Acad. Sci. USA.* 88:517–521.